Department of Applied Mechanics

Strength of rough interfaces

A micro-scale approach to steel-epoxy and composite systems

Mikko Kanerva

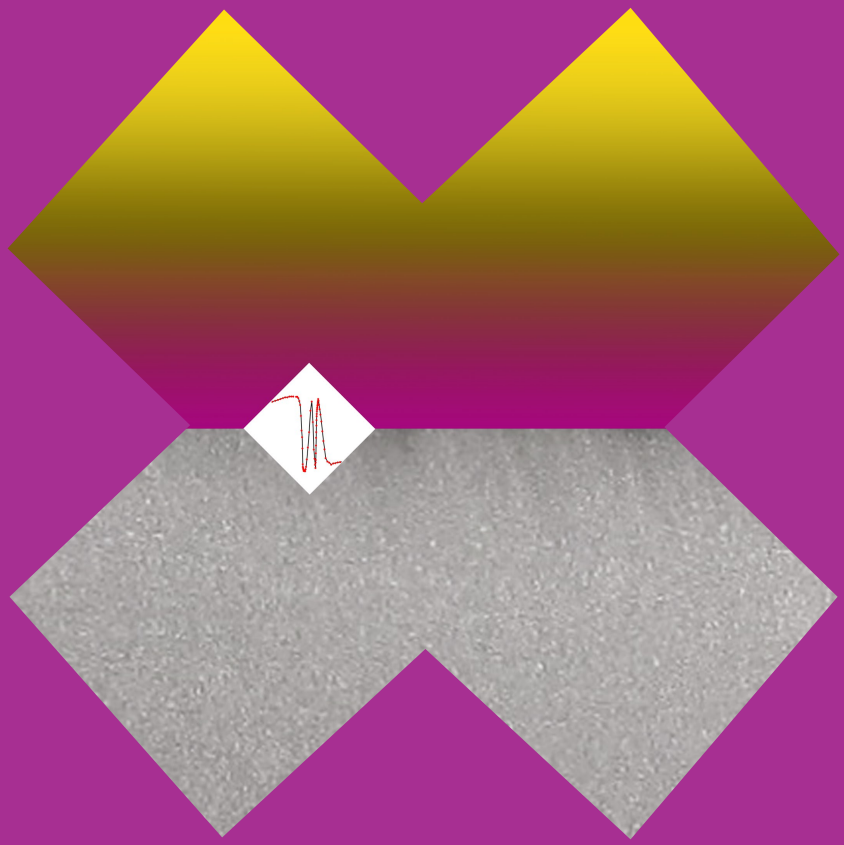

Aalto University

DOCTORAL DISSERTATIONS

Aalto University publication series
DOCTORAL DISSERTATIONS 151/2014

Strength of rough interfaces

A micro-scale approach to steel-epoxy and composite systems

Mikko Kanerva

A doctoral dissertation completed for the degree of Doctor of Science (Technology) to be defended, with the permission of the Aalto University School of Engineering, at a public examination held at the lecture hall 216 of the school on 21 November 2014 at 12.

Aalto University
School of Engineering
Department of Applied Mechanics

Supervising professor
Professor Jukka Tuhkuri

Thesis advisor
Professor Olli Saarela

Preliminary examiners
Professor Vladimír Cech
Brno University of Technology, Czech Republic

Professor Hiroyuki Hamada
Kyoto Institute of Technology, Japan

Opponent
Associate Professor Christian Berggreen
Technical University of Denmark, Denmark

Aalto University publication series
DOCTORAL DISSERTATIONS 151/2014

ISBN 978-952-60-5890-0
ISBN 978-952-60-5891-7 (pdf)
ISSN-L 1799-4934
ISSN 1799-4934 (printed)
ISSN 1799-4942 (pdf)
http://urn.fi/URN:ISBN:978-952-60-5891-7

Unigrafia Oy
Helsinki 2014

Finland

441 697
Printed matter

Aalto University

Abstract

Aalto University, P.O. Box 11000, FI-00076 Aalto www.aalto.fi

Author
Mikko Kanerva

Name of the doctoral dissertation
Strength of rough interfaces:
A micro-scale approach to steel-epoxy and composite systems

Publisher School of Engineering

Unit Department of Applied Mechanics

Series Aalto University publication series DOCTORAL DISSERTATIONS 151/2014

Field of research Mechanics of Materials

Manuscript submitted 17 March 2014 **Date of the defence** 21 November 2014

Permission to publish granted (date) 19 May 2014 **Language** English

☐ **Monograph** ☒ **Article dissertation (summary + original articles)**

Abstract

The load-carrying capability of current multi-component materials is highly dependent on the performance of interfaces. This thesis studies the mechanical strength of planar interfaces and focuses on the effects of microscopic roughness.

The first part of the thesis concentrates on a stainless steel-epoxy bi-material. The effect of the preparation at an elevated temperature is studied by analysing the residual stress state using an X-ray diffraction method. The bi-material's interface strength is determined on the basis of the energy release rate (G_c) and particular attention is paid to advancing the notched coating adhesion (NCA) test method. A systematic pre-crack preparation technique and a definition for the critical point of the interface collapse are developed in order to obtain a representative G_c and also to distinguish the effects of the substrate morphology. In this work, grain boundary grooves with a depth of 1-2 microns were found to produce the highest G_c values. A stabilizing aging effect was observed to reduce the interface strength. A finite element model was generated based on atomic-force microscopy and mode II dominated crack growth was simulated on a micro-scale. The simulation revealed an M-shaped crack-tip mode-mixity distribution for the interface at grain boundary grooves and a 100-fold toughening effect; however, the toughening effect decreased 35% due to modelled voids at the grain boundaries.

The second part of the thesis concentrates on planar interfaces in composite systems. A literature review was conducted to review the various effects of roughness patterns due to peel ply surface treatments. An experimental study focuses on overlaminated interfaces in a glass-fibre-reinforced, unsaturated polyester composite. It was found that a combination of moisture and elevated temperature cause a significant decrease in the interface strength and durability of composites pre-treated using either polymeric peel plies or an impregnated tear ply.

The work produced a model of a series of experiments, which can be used to describe the essential factors of strength for stainless steel-epoxy interfaces. The thesis concludes that a rough metal-polymer interface can be successfully analysed on a micro-scale when residual stresses, substrate morphology and flaws are realistically incorporated. The developed simulation scheme can be used to interpret the influence of groove-type micro-roughness on macroscopic performance. Also, an experimental study was conducted to offer a baseline for future simulations of systematically roughened, composite-composite interfaces.

Keywords interface, micromechanics, fracture, composite

ISBN (printed) 978-952-60-5890-0 **ISBN (pdf)** 978-952-60-5891-7

ISSN-L 1799-4934 **ISSN (printed)** 1799-4934 **ISSN (pdf)** 1799-4942

Location of publisher Helsinki **Location of printing** Helsinki **Year** 2014

Pages 97 **urn** http://urn.fi/URN:ISBN:978-952-60-5891-7

Tekijä
Mikko Kanerva

Väitöskirjan nimi
Karheuden vaikutus rajapinnan lujuuteen:
Teräs-epoksi- ja komposiittiyhdistelmien tarkastelu mikrotasolla

Julkaisija Insinööritieteiden korkeakoulu

Yksikkö Sovelletun mekaniikan laitos

Sarja Aalto University publication series DOCTORAL DISSERTATIONS 151/2014

Tutkimusala Lujuusoppi

Käsikirjoituksen pvm 17.03.2014 **Väitöspäivä** 21.11.2014

Julkaisuluvan myöntämispäivä 19.05.2014 **Kieli** Englanti

☐ **Monografia** ☒ **Yhdistelmäväitöskirja (yhteenveto-osa + erillisartikkelit)**

Tiivistelmä

Materiaaliyhdistelmien kuormankantokykyyn vaikuttavat suuresti komponenttien väliset rajapinnat. Tämä väitöskirja tutkii tasomaisten rajapintojen lujuutta ja pinnan morfologian vaikutusta murtumiskäyttäytymiseen mikrotasolla.

Väitöskirjan ensimmäinen osio keskittyy ruostumattomasta teräksestä ja epoksiliimasta muodostettuun bi-materiaaliin. Materiaalin valmistaminen korotetussa lämpötilassa johtaa sisäisiin jäännösjännityksiin, joita tutkitaan röntgensäteiden diffraktioon perustuvalla menetelmällä. Rajapinnan murtositkeys (G_c) määritellään vapautuvan deformaatioenergian perusteella. Kokeellista menettelyä G_c-arvon määrittämiseksi kehitetään tarkan esisärön valmistusmenetelmän ja kriittisen, rajapinnan äkkinäiseen pettämiseen johtavan venymätason määrittelyn avulla. Tutkimuksessa todetaan 1-2 mikrometriä syvien raerajauurteiden johtavan korkeampiin G_c-arvoihin verrattuna elektrolyyttisellä kiillotuksella tai etsauksella aikaansaatuun morfologiaan. Murtositkeys tutkituilla rajapinnoilla alenee ajan funktiona, mutta stabiloituu lopulta. Raerajauurteiden vaikutusta tutkitaan elementtimenetelmällä muodostamalla rajapinnan geometriamalli atomivoimamikroskoopilla tehtyjen mittausten perusteella. Simulaatio rajapinnan murtumisesta osoittaa raerajauurteen aiheuttavan M-muotoisen särön kärjen kuormitusmoodijakautuman ja 100-kertaisen sitkeytymisefektin. Tämä efekti pienenee 35 %, mikäli raerajauurteisiin mallinnetaan adheesiovikoja.

Väitöskirjan toinen osio keskittyy tasomaisiin rajapintoihin kuitulujitetuissa komposiiteissa. Tutkimus aloitetaan kirjallisuusselvityksellä, jonka tavoitteena on selvittää systemaattisen karheuden vaikutusta liimattujen ja laminoitujen liitosten ominaisuuksiin. Kokeellinen työ keskittyy lasikuidulla lujitetun polyesterilaminaatin pintakäsittelyyn karhennuskankaiden avulla. Tulokset osoittavat, että kosteuden ja korotetun lämpötilan yhteisvaikutus alentaa huomattavasti polymeeripohjaisilla karhennuskankailla esikäsiteltyjen liitosten lujuutta.

Väitöskirjatyön tulos on kokeisiin pohjautuva proseduuri, jolla voidaan määrittää ruostumattoman teräksen ja epoksiliiman rajapinnan murtositkeyteen oleellisesti vaikuttavat tekijät. Koetulosten perusteella voidaan edelleen simuloida mikroskooppisen karheuden vaikutus rajapinnan mekaaniseen suorituskykyyn makroskaalassa. Tulokset osoittavat, että karheuden vaikutus rajapinnan murtumiseen voidaan simuloida, mikäli jäännösjännitykset, morfologia ja adheesioviat otetaan mallinnuksessa huomioon realistisesti.

Avainsanat rajapinta, mikromekaniikka, murtuminen, komposiitti

ISBN (painettu) 978-952-60-5890-0 **ISBN (pdf)** 978-952-60-5891-7

ISSN-L 1799-4934 **ISSN (painettu)** 1799-4934 **ISSN (pdf)** 1799-4942

Julkaisupaikka Helsinki **Painopaikka** Helsinki **Vuosi** 2014

Sivumäärä 97 **urn** http://urn.fi/URN:ISBN:978-952-60-5891-7

Preface

The work for this dissertation has been an interesting but long journey. I feel gratefulness to my opponent Dr. Christian Berggreen and pre-reviewers Dr. Vladimír Čech and Dr. Hiroyuki Hamada for making the finishing respectable. I thank my supervising professor Jukka Tuhkuri for his guidance with the review process of my dissertation and my advising professor Olli Saarela for reading all the numerous versions of article manuscripts. I would like to acknowledge Oy Kromatek AB, Outokumpu, Andritz Automation and Cytec for the contribution to my research work. Also, I thank Dr. L-S. Johansson and Dr. J.M. Campbell for the XPS work. I cheer on my colleagues at the KRT laboratory for their help.

One of my colleagues has kept surprising me time and again. Dr. Essi Sarlin has been an irreplaceable aid during the entire process. Not a single time she said no to my ideas of further studies, new microscopy samples and new test specimens. Also, her critical attitude was of great help when publishing research results. Thank you Essi for help and for being a wonderful colleague.

I believe that much of my efforts and achievements are due to the great personal connections I have; I owe much to the closest people around me. Frequently I needed someone to remind me that there is another life outside the laboratory and engineering. I want to thank my friends Pasi, Fumie, Ritva, Sirkka-Liisa, Ozgur, JP, Satu and Jouko, and naturally my dear sisters Saija and Marju, for reminding me of the real world.

Experiences with wonderful people have prepared me for many challenges that I have went through. Without an iron will for destroying continuous difficulties and barricades I would not have succeeded. For the iron will, I thank the brothers J. and J. Tiihonen, for the great model of fighting for one's dreams.

The journey towards being an academic researcher has indisputably increased my mental toughness. However, just as for the strongest materials, toughness does not necessarily imply great hardness but instead a specific composition with soft phases. The logic and rationale needed for a research work are fed and balanced by creativity and empathy. Therefore, I thank the women of my younger years, Tiina and Inka, for teaching me what is the kindness and empathy in the human mind and heart. And Anna, you offered me a puzzle, which I will learn one day—thank you.

The courage to face challenges has been an undeniable advantage during the work. In my case, the courage stems from a place deep inside of me. Specifically, I believe that it is due to the firm family relations I have always had. I am grateful for the care to the family Toivanen, with whom I have spent a great deal of my youth. Thereby I learned to see, and do, many things, even fundamentals, in more than one way. Moreover, the core of my courage is the time spent with my best friend Juha Toivanen. Juha, your faithfulness and positive attitude towards me have definitely made me me. I will be obliged forever for the years we have spend together.

Most sincerely, I am of what I was made of. Therefore, more than anything in this world, I thank my parents Markku and Leena Kanerva. You brought me up to take chances; you encouraged me to choose what I felt is right and to live my life my way. You have taught me to be unprejudiced to new ideas, new people and new perspectives. How can I ever show enough gratitude for your warmth and paving the way for my development?

The corner stone of my understanding of the family life—a safe, firm and nourishing home—is the presence of grandparents. To realize that I cannot have them all here now, must be the lesson of the present day's importance. Still, I have the memories to remind me—the memories will work as a guide from now on.

Tanya, my love, with you I want to walk towards the future.

Last but absolutely not least I thank God for the divine abilities to love and to be creative.

Hereby I want to encourage all researchers and the future generations of doctoral students to neglect pessimists' comments and to believe in yourselves when your intuition tells you an idea.

"Who says we need the top wing? Who says we need anything?"

Howard Hughes, in the movie The Aviator, when developing his phenomenal monoplane

Otaniemi, Finland, October 3, 2014,

Mikko Kanerva

Contents

Preface **1**

Contents **5**

List of Publications **9**

Author's Contribution **11**

1. Introduction **17**

1.1 Objectives and scope 18

1.2 Material systems studied 20

2. Background and the state of the art **23**

2.1 Challenge of roughness 23

2.1.1 Model interfaces 23

2.1.2 Gradient interfaces: Interphases 25

2.1.3 Wetting of surfaces 27

2.2 The measuring of interface strength 27

2.2.1 Challenge of interface strength 28

2.2.2 Fracture testing 29

2.2.3 Hygrothermal aging 32

2.3 Simulation of interface fracture on a micro-scale 33

2.3.1 Limits of continuum formulation 33

2.3.2 Challenge of gradual fracture 35

3. Methods and conducted work **39**

3.1 Methods 39

3.1.1 Single-lap shear test 39

3.1.2 Wedge test 39

3.1.3 Double cantilever beam test (DCB) 40
3.1.4 Notched coating adhesion test (NCA) 41
3.1.5 Profilometry 42
3.1.6 Acoustic emission measurement (AE) 42
3.1.7 Differential scanning calorimetry (DSC) 43
3.1.8 X-ray diffraction surface stress measurement (XRD) 43
3.1.9 Field-emission scanning electron microscopy (FESEM) 44
3.1.10 X-ray energy dispersive spectroscopy (EDS) 44
3.1.11 X-ray photoelectron spectroscopy (XPS) 45
3.1.12 Atomic force microscopy (AFM) 45
3.1.13 Analytical residual stress estimation 47
3.1.14 Finite element analysis (FE) 47
3.1.15 Virtual crack closure technique (VCCT) 47
3.2 Interface strength at a metal-polymer interface:
Work conducted in Publications I–III 48
3.2.1 Surface condition of AISI 304 based on the existing literature 48
3.2.2 Control of the substrate surface condition for the thesis experiments 49
3.2.3 Residual stresses at bi-material interfaces 52
3.2.4 Fracture test method development 52
3.2.5 Variation in critical energy release rate values 56
3.2.6 Description of the fracture process 58
3.3 Simulation of fracture along an interface with micro-roughness:
Work conducted in Publication IV 59
3.3.1 Interface model 59
3.3.2 Gradual fracture along micro-roughness 62
3.3.3 Engineering toughening factor 65
3.4 Strength of composite-composite interfaces:
Work conducted in Publications V–VI 65
3.4.1 The peel ply surface treatment of composites: A literature review 66
3.4.2 Modification of composite-composite interfaces for the thesis experiments 70
3.4.3 Static strength and durability 75

4. Summary and conclusions **77**
4.1 Strength of rough stainless steel-epoxy interfaces 77

4.2 Strength of rough composite-composite interfaces 80
4.3 Conclusions 82

Bibliography **85**

Publications **95**

List of Publications

This thesis consists of an overview and of the following publications which are referred to in the text by their Roman numerals.

I M. Kanerva and O. Saarela. X-ray diffraction and fracture based analysis of residual stresses in stainless steel–epoxy interfaces with electropolishing and acid etching. *International Journal of Adhesion and Adhesives*, Volume 39, pages 60–67, 2012.

II M. Kanerva, E. Sarlin and O. Saarela. Variation in mode II dominated interface fracture of stainless steel-epoxy bonds. Part 1: Mechanical testing. *Engineering Fracture Mechanics*, Volume 99, pages 147–158, 2013.

III M. Kanerva, E. Sarlin, J.M. Campbell, K. Aura and O. Saarela. Variation in mode II dominated interface fracture of stainless steel–epoxy bonds. Part 2: Multi-scale damage analysis. *Engineering Fracture Mechanics*, Volume 97, pages 244–260, 2013.

IV M. Kanerva, J. Jokinen, E. Sarlin and O. Saarela. Crack propagation under mode II dominance at stainless steel–epoxy interfaces with residual stresses and micro-scale roughness. *International Journal of Solids and Structures*, Volume 50, pages 3399–3405, 2013.

V M. Kanerva and O. Saarela. The peel ply surface treatment for adhesive bonding of composites: A review. *International Journal of Adhesion and Adhesives*, Volume 43, pages 60–69, 2013.

VI M. Kanerva, E. Sarlin, K. Rämö, O. Saarela. Durability and interphases in adhesively bonded epoxy-polyester interfaces. In *Proceedings of the International Conference on Composite Materials*, ISBN 978-0-9696797-1-4, held in Montreal, Canada, pages 7614–7626, July 28 - August 2, 2013.

Author's Contribution

Publication I: "X-ray diffraction and fracture based analysis of residual stresses in stainless steel–epoxy interfaces with electropolishing and acid etching"

The author wrote the article, interpreted the results, performed all of the mechanical tests and is the corresponding author. Prof. O. Saarela revised the article. All XRD measurements were performed by T. Kiesi, M. Hakanen and S. Papula.

Publication II: "Variation in mode II dominated interface fracture of stainless steel-epoxy bonds. Part 1: Mechanical testing"

The author wrote the article, interpreted the results, performed all of the mechanical tests and is the corresponding author. E. Sarlin performed all of the FESEM imaging and helped write the article. Prof. O. Saarela revised the article.

Publication III: "Variation in mode II dominated interface fracture of stainless steel–epoxy bonds. Part 2: Multi-scale damage analysis"

The author wrote the article, interpreted the results, performed all of the AFM measurements and is the corresponding author. E. Sarlin performed all of the FESEM imaging and the EDS analysis and helped interpret the results. J.M. Campbell performed all XPS work and helped write the article. K. Aura performed all AE measurements. Prof. O. Saarela revised the article.

Publication IV: "Crack propagation under mode II dominance at stainless steel–epoxy interfaces with residual stresses and micro-scale roughness"

The author wrote the article, interpreted the results, developed the FE model, performed all of the AFM measurements and is the corresponding author. J. Jokinen helped develop the FE model and also helped write the article. E. Sarlin performed the FESEM imaging. Prof. O. Saarela revised the article.

Publication V: "The peel ply surface treatment for adhesive bonding of composites: A review"

The author composed the article and is the corresponding author. FESEM imaging was performed by E. Sarlin. Prof. O. Saarela revised the article.

Publication VI: "Durability and interphases in adhesively bonded epoxy-polyester interfaces"

The author wrote the conference article, interpreted the results, performed all of the mechanical tests and is the corresponding author. E. Sarlin performed all of the FESEM imaging and the EDS analysis and helped with the mechanical tests. K. Rämö conducted the DSC measurements. Prof. O. Saarela revised the article.

Nomenclature

Variables & Symbols

A	Fracture surface (projection) area
a	Crack length (momentary)
b	Specimen width
E	Young's modulus
F	Large-displacement correction factor (see ISO 15024 standard)
G	Strain energy release rate upon fracture
G_{II}	Mode II energy release rate
G_I	Mode I energy release rate
G_a	Apparent critical energy release rate
G_c	Critical mixed mode energy release rate (at the time of interface collapse)
G^{Ξ}	Critical energy release rate omitting toughening mechanisms
h	Thickness of the delaminating layer upon fracture
L	Load (tensile and opening)
N	Load block correction factor (see ISO 15024 standard)
P_{avg}	Power released by crack-tip during stable propagation
t	Adherent thickness

T_g	Glass transition temperature
U_1	Total transferred energy (into a closed system)
U_2	Irreversibly dissipated energy upon fracture
U_3	Stored elastic and thermal energy upon fracture
U_4	Kinetic energy upon fracture
v_t	Crack-tip velocity during stable propagation
W_f	Fracture energy
$W_{0,a/c}$	Work of adhesion per fracture surface area '*A*', related to either adhesion (*a*) or cohesive (*c*) failure
Y	Crack opening displacement
γ_i	Surface energy of material *i*
γ_{12}	Interfacial free energy for materials *1* and *2*
Δ	Crack length correction term (see ISO 15024 standard)
Ψ	Miscellaneous energy dissipation upon fracture, undefinable by γ_i
δ	Displacement at the load line
ε	Critical (longitudinal) mechanically induced strain
ε_0	Bi-axial residual strain (in the delaminating layer)
ν	Poisson's ratio of delaminating material
ν_s	Poisson's ratio of substrate material
σ_0	Bi-axial residual stress (in the delaminating layer)
ψ	Fracture mode-mixity in two dimensions, ψ = atan(G_{II}/G_I)

Acronyms

AFM	Atomic force microscopy
AE	Acoustic emission (measurement)
CTE	Coefficient of linear thermal expansion

DCB	Double cantilever beam (test)
DSC	Differential scanning calorimetry
EDS	X-ray energy dispersive spectroscopy
ENF	End-notched flexure (test)
FE	Finite element (analysis)
$FESEM$	Field-emission scanning electron microscopy
IPN	Interpenetrated (molecule) network
NCA	Notched coating adhesion (test)
RH	Air relative humidity
RT	Room temperature
$SIMS$	Secondary-ion mass spectroscopy
UP	Unsaturated polyester
$VCCT$	Virtual crack closure technique
XPS	X-ray photoelectron spectroscopy
XRD	X-ray diffraction surface stress measurement

1. Introduction

Interfaces are often seen as strict geometric boundaries between unlike components. However, interfaces are more than the sum of the features represented by the two facing components. Interaction between the components plays a crucial part. In modern composite and hybrid materials, interfaces are expected to bring out synergetic effects; in addition, they should enable the tailored mixture of two or more unlike components in a single united system.

Interfaces can be found in almost every material, excluding pure amorphous solids, but the characteristic length scale can range from a few nanometers to several millimeters. One example of an engineering material that involves several interfaces over a broad range of length scales, is a hybrid laminate composed of monolithic metal sheets and a fibre-reinforced composite material, as shown in Fig. 1.1. The metal sheets and the composite are clearly united by an interface. Secondly, the composite part is composed of several layers, with different orientations, and they are united by interfaces. Third, the reinforcing fibres and the surround-

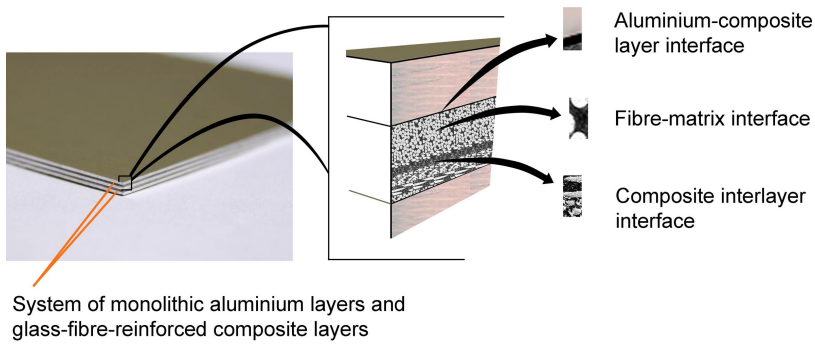

Figure 1.1. Hybrid laminate is a type of engineering material that has a multi-length scale structure and several different interfaces between its components.

ing plastic are united by an interface. The list could be expanded further, towards an atomic scale.

Interfaces make an important contribution to the load-carrying characteristics of engineering materials. For example, the trend in the field of adhesive bonding is not only to adjust the substrate surface chemistry but also to optimize the substrate roughness. In particular, the adhesion at the interfaces can be enhanced by creating pre-determined roughness shapes so that the characteristic size of these roughness shapes is only a few micrometres. Experimental studies on the adhesion and controlled roughness shapes have been reported by, for example, Roy et al. (2007), Kim et al. (2010) and Song et al. (2011). Likewise, numerical simulations of model interfaces have been reported by Zavattieri et al. (2007), Reedy (2008) and Tvergaard and Hutchinson (2009). In addition to the engineering fields, the importance of optimum surface morphologies has been reported in studies dealing with medical applications, for example in those related to the growth of bone on metallic implants (Cooper, 2000). Efficient design and optimization using computer simulations necessitate data on the mechanical behaviour of interfaces in order to model microscopic de-adhesion processes.

1.1 Objectives and scope

The current challenge in research on rough interfaces is that there is not enough knowledge about the numerous microscopic de-adhesion processes. The objective of this thesis is to concentrate on the influence of microscopic roughness and present new information as well as solutions for analysing interface strength. Because of the wide range of length scales related to engineering materials, it is necessary to highlight the perspective of this thesis: the thesis concentrates on engineering materials designed for load-carrying applications. Interfaces in these materials are considered on a micro-scale and the property of interest is the strength with respect to external mechanical loading. The term 'micro-scale' refers to details ranging from approximately 100 nm to 500 microns in size. Also, the work in the thesis can be divided into two parts based on the material systems studied, namely:

1. *Stainless steel-epoxy interfaces*;

2. *Composite-composite interfaces*.

The work consists of six publications in total (Publications I–VI), each of which has its own set of objectives, or 'problems', as described in Tables 1.1 and 1.2.

Table 1.1. Reporting and methods for solving the respective challenges presented in the first part of the thesis.

Research problem	Reporting and methods
How to determine residual stresses at different steel-epoxy interfaces at a micrometre accuracy?	Publication I: Experimental analysis - XRD measurements on steel, at the steel-epoxy interface - Analytical modelling of the stress (strain) distribution - Strength study by an indentation method
How to determine accurate measures of strength for rough steel-epoxy interfaces? How to study the effect of microscopic substrate surface morphology? How to describe the fracture processes on different length scales when a crack grows along a rough steel-epoxy interface?	Publication II: Experimental analysis - Control of the steel surface morphology - NCA fracture testing of interfaces and determination of critical strain energy release rate values per interface configuration - Advancement of the NCA method in terms of the definition of the critical point Publication III: Experimental analysis - AFM and FESEM analysis of the substrate and fracture surfaces - EDS and XPS chemical analysis of the fracture surfaces to study the fracture loci - AE measurement of the fracture process
How to simulate a macro-scopic structure with an interface having microscopic details? How does mode II dominated fracture progress along rough interfaces?	Publication IV: Numerical analysis - Simplification of steel-epoxy interface for a finite element model and simulation - Modelling of micro-roughness at interface - Simulation of mode II predominated crack propagation using the VCCT method

The thesis consists of a literature survey and a report on the essential findings and results of the thesis. The literature survey is presented in Chapter 2. The objective of the literature survey is to describe (1) the interface as a structural concept, (2) the challenges of measuring inter-

face strength and (3) the current state of the art of simulating flaws at interfaces based on the existing literature. After the literature survey, Chapters 3–4 focus on the applied research methods, on the work and results presented in Publications I–VI and also on the final conclusions.

Table 1.2. Reporting and methods for solving the respective challenges presented in the second part of the thesis.

Research problem	Reporting and methods
How do peel ply treatments affect composite surfaces? How does the morphology and surface chemistry after a peel ply treatment affect the resulting interface strength?	Publication V: Literature-based analysis - Literature review based on research articles and conference publications on the peel ply surface treatments
Can a tear ply (with an epoxy-based impregnation resin) be used for modifying composite-composite interfaces? How sensitive are peel ply pre-treated interfaces to moisture-temperature effects?	Publication VI: Initial experimental analysis - Shear strength testing for a screening study - EDS and FESEM for studying the interface composition and structure - DSC for studying epoxy-polyester interaction - Steel mesh treatment for studying the effect of peel ply raw material on interface strength - Fracture testing for a durability study

1.2 Material systems studied

In this thesis, the term *material system* refers to either a bi-material or a layered multi-material system (i.e. composite). Accordingly, the thesis concentrates on two conceptually distinguishable examples of structural interfaces. In the first part of the thesis, a stainless steel-epoxy interface is studied. The components at the interface are as follows:

- The substrate alloy is AISI 304 austenitic stainless steel, provided by Outokumpu, Finland.

- The adhering polymer is an *FM® 300 U* unsupported epoxy film adhesive, provided by Cytec Engineered Materials, USA.

In the second part of the thesis, a composite-composite interface is studied; hence, the substrate and the adhering composite are of the same material. The components of the composite material are as follows:

- The reinforcing fibres are E-glass, sized fibres (*EDR17-2400-386* unidirectional fibre and *M501* mat fabric), provided by Jushi Group Co., China, and Ahlstrom, Finland, respectively.

- The composite's matrix resin is *Aropol M300 TBR* unsaturated polyester, provided by Ashland Composite Polymers, USA.

In this text, the term *polymer* refers to a hydrocarbonous, cross-linking polymeric substance with a high molecular weight. The term *epoxy* refers to a polymer that is mainly composed of bisphenol and epichlorohydrin. *Unsaturated polyester* in this text refers to a polymer that is mostly based on orthophtalic resin, styrene monomer diluent and a mixture of peroxide co-reactants (initiators). Usually, orthophtalic resins refer to blends of phathalic anhydrides, maleic anhydrides and glycols (Malik et al., 2000). In addition to mixtures of monomers, pre-polymers and co-reactants, commercial polymers can include cure inhibitors, fire retardants, waxes and plasticizers (Neumann, 1981). In particular, commercial epoxies are blends of specific types of bisphenols and several different pre-polymers and co-reactants; they include aminophenols, glycidyl derivatives and polyamines.

2. Background and the state of the art

2.1 Challenge of roughness

2.1.1 Model interfaces

Let us start by imagining a model interface—represented by a straight line (or a flat plane) between two homogenous materials. The distinction, whether the two materials are actually separate or united by the interface, can be handled using the concept of surface free energy. Mechanical de-adhesion of two united materials leads to the instant formation of new free surfaces. The formation of surfaces occurs through molecular-scale re-arrangement, which consumes energy. The energy consumed by the formation of surfaces shall be called fracture energy. A straightforward equation for the fracture energy, W_f, of an interface can be expressed as follows (e.g. Packham, 2003):

$$W_f = W_0 + \Psi, \tag{2.1}$$

where W_0 is the work of adhesion per fracture surface (projection) area, and the term Ψ represents miscellaneous energy dissipation processes other than those defined by the surface energies (e.g. plasticity). The term W_0 can be calculated using either of the following equations:

$$W_{0,a} = \gamma_1 + \gamma_2 - \gamma_{12}, \tag{2.2}$$

$$W_{0,c} = 2\gamma_1, \tag{2.3}$$

where γ is the surface energy, the sub-indexes *1* and *2* refer to the two bonded materials, and the sub-indexes a and c refer to adhesive and cohesive fracture (of material *1*), respectively. The term γ_{12} is the so-called

interfacial free energy and refers to the decrease in the free energy due to molecular-scale interaction or re-orientation at the interface during bonding. The term γ_{12} basically represents the issues for an interface that are not just the sum of the features represented by the two facing materials.

Surface energy (γ) is often being compared to surface tension—based on the experimental determination defined for an ideally flat surface. In spite of the experimental difficulties of determining absolute surface energies at real interfaces (see, e.g. Baldan, 2004; Giese et al., 1996), Equation 2.1 illustrates the essence of roughness-induced increases in strength at micro-scale interfaces. Interfaces in practical material systems are formed on relatively rough substrates, and the geometric shapes dividing the two bonded materials can be complicated or even fractal (Charkaluk et al., 1998). Roughness on a substrate surface refers to an increased true surface area, increased diffusion and also increased molecular-scale contacts per projection area. A sharp shape, such as an oxide spike's tip, represents a higher atomic-level surface energy when compared to a perfectly flat crystal lattice and, thereby, it is expected to assist chemical reactions and enhance bond formation. For real interfaces, the value of W_0 is typically low and the term Ψ mostly contributes to the fracture energy (Packham, 1986; Janarthanan et al., 1997).

The effect of surface shapes on a molecular scale has been found to affect the nature of polymer-facing interfaces through ordering and packing of molecular entities and friction (Johnston and Harmandaris, 2013). Precise roughness shapes, which form the *morphology* of substrate surfaces, have been studied and there have been attempts to calculate the share of roughness shapes with respect to interface strength (Gent and Lin, 1990; Sargent, 1994). In these studies, the share has been addressed to either increased surface area or mechanical interlocking. Mechanical interlocking refers to the idea of cavity-type roughness shapes filled by the adhesive (resin) during bonding. These early studies assumed model roughness shapes and relied on the idea of ultimate stress or the work of adhesion. Recently, fracture mechanics and numerical methods have been applied to studies on the effects of roughness on interface strength (Reedy et al., 2007; Zavattieri et al., 2008). Consequently, the roughness effect on interface strength in general has been termed the *toughening effect* in the existing literature. The usual phenomenon 'producing' a toughening effect upon fracture is called *crack tip shielding*. Crack-tip shielding in general can refer (1) to specific crack path meandering and the following

closure of the crack tip, (2) to bridging of the crack tip or (3) to the production of elastically constrained zones around the crack tip (Ritchie, 1988, 2011).

2.1.2 Gradient interfaces: Interphases

An interface does not need to refer to a discrete boundary. *Gradients* can be observed at real interfaces, meaning that the composition or value of one mechanical property is gradually transformed into another value. A gradient can be defined by, for example, the chemistry (e.g. the polymeric network structure) or stiffness (e.g. Young's modulus) at the interface (Prikryl et al., 2003; Possart et al., 2006; Jancar, 2008). The correct, or appropriate, representation of the gradient depends on the aim of the study in question. For example, the gradient represented on a compositional basis can have a specific geometric representation but it might not match the gradient represented on a stiffness basis. The reason for this is that there can be a third party at the interface. That is to say, the substrate material tends to react with the adhering material so that an *interphase* forms.

Gradient interfaces have also been modelled in the existing literature; various representations of gradient interfaces have been investigated for numerical computer simulations (Shbeeb and Binienda, 1999; Yang and Pitchumani, 2004; Papanicolaou et al., 2009).

Metal-polymer systems

Based on the existing literature, interphases at metal-polymer interfaces have been observed for aluminium, copper, gold and titanium substrates coated with different epoxies. Bentadjine et al. (2001) observed a lowered glass transition temperature (T_g) for thin epoxy coatings (0–0.5 mm above interface) on either chemically etched titanium or chemically etched aluminium substrates. Additionally, less amine co-reactant conversion was observed for the chemically etched titanium substrate and very thin coatings. Bentadjine et al. (2001) suspected the presence of dissolved oxide- or hydroxide-metallic surface species. Possart et al. (2006) discovered slower curing and also a lower final degree of cure in very thin epoxy coatings (100–200 nm) on aluminium, copper and gold substrates. Possart et al. (2006) studied the stiffness distributions in the coatings and determined interphases with thicknesses varying between approximately 70 µm and 120 µm. Bouchet et al. (1999) in turn studied the mechani-

cal properties of interphases on aluminium substrates by calculating an 'equivalent' Young's modulus for a coated specimen using a flexure test; the determined distributions of the equivalent Young's modulus showed significantly higher values near the interface (compared to bulk) and indicated an interphase with a thickness of approximately 150–200 μm. The increase in the values of continuum properties, such as Young's modulus, at interfaces, has been explained (for epoxy-amine systems) in terms of a considerable concentration of organo-metallic complexes, which result in needle-like crystal formations and, consequently, in a reinforcing effect (Bentadjine et al., 2001; Aufray and Roche, 2006).

Polymer-polymer systems

For polymer-polymer systems, contact between two polymers can lead to a full or partial healing (i.e. disappearance of the interface). Typical analysis of the thermodynamics of polymer systems has been based on the Flory-Huggins theory and polymer-solvent interaction parameters (Sperling, 2006). Moreover, the molecular compatibility between two cross-linking polymers depends on the curing kinetics, molecular mobility and possible catalytic reactions. For example, the compatibility between epoxy resins and unsaturated polyesters has been studied in the existing literature (Lin and Chang, 1992). On a molecular scale, the resulting polymer structure is an interpenetrated network (IPN), although the level of interpenetration and network homogeneity are dependent upon the cure temperature, resin stoichiometry and a certain molecular interlocking mechanism (Lin et al., 1995; Shih and Jeng, 2004). The mechanical performance of IPNs has also been studied and it has been found that, similarly as for interpenetration, the mechanical toughness of the resulting polymer depends greatly on the stoichiometry during the mixing of the resins (Lin et al., 1999).

Because of their ability to interact during the cross-linking reactions, practical polymer systems are usually characterized at the 'full' degree of cure. For a fully cured substrate, the interface formation is determined by the adhesive's diffusion and wetting characteristics. The smallest adhesive's species might be able to penetrate into the cross-linked substrate, which leads to a deviation in resin stoichiometry above the bond line. In particular, the diffusion of co-reactant species can be problematic since it makes the bond formation substrate dependent and also can make the quality of the bond line time dependent (Cognard, 2006).

2.1.3 Wetting of surfaces

The approach in Eq. 2.1 can be presented the other way around: two separate surfaces can be brought together to form a sound solid. When combining a solid substrate and a cross-linking adhesive component, sufficient wetting of the substrate surface by the adhesive is necessary. The wetting phenomenon is governed by the surface energy relation between the substrate and adhesive as well as by the ability of the adhesive to flow (Adamson, 1990; Baldan, 2004). Easy flowing of the polymer prefers a low viscosity and low level of cross-linking; gelled thermosetting polymers and thermoplastics near their glass transition temperature, e.g. film adhesives and pressure sensitive adhesives, respectively, require external pressure in order to flow. Roughness of the substrate surface can increase the substrate's surface free energy but also prevent the adhesive to flow throughout the morphology; air might get trapped in surface asperities and form voids, namely adhesion flaws (Persson and Tosatti, 2001; Baldan, 2012).

The wetting characteristics of a surface are studied using contact angle measurements for determining surface tension. The well-known Young's equation is used for relating contact angle data and surface tension (Baldan, 2012). The surface tension equilibrium at a surface-fluid interface can be further analysed to incorporate specific forces, e.g. due to polar Lewis acid-base interaction (Van Oss, 1987) and dispersive Lifshitz-van der Waals interaction (Van Oss, 1988). However, it has been argued whether or not contact angle data using certain probe liquids can characterize the behaviour of commercial polymer systems, where surface tension is highly dependent on the temperature, degree of cure and particulate toughening (Chin and Wightman, 1996; Flinn et al., 2007; Móczó et al., 2012).

2.2 The measuring of interface strength

This chapter will discuss and review the challenges in defining interface strength, the means for experimental determination and the dependence of interface fracture on the pre-crack preparation, crack-tip loading modes and aging.

2.2.1 Challenge of interface strength

During the course of developing numerical methods, such as the finite element method (FE), interface strength has been mostly considered on an energy transformation basis rather than a stress basis (Evans, 2006). Incremental failure of an interface can be understood to release a specific amount of energy, ΔU. Furthermore, the strain energy release rate, G, refers to a fraction of 'subjected' or 'transferred' energy, $U_1 = U_2 + U_3 + U_4$ (e.g. due to the mechanical work done by an external force), per fracture surface area:

$$G = \frac{dU_1}{dA} - \frac{dU_3}{dA}, \tag{2.4}$$

where U_1 is the transferred energy, U_3 is the stored (elastic and thermal) energy and A is the fracture surface (projection) area in the system at the time of observation. During quasi-static testing, thermal (stored) energy and the amount of kinetic energy (U_4) can be assumed negligible and, therefore, the fraction $U_1 - U_3$ essentially corresponds to the irreversibly dissipated energy (U_2), e.g. due to the formation of new (fracture) surfaces. The strain energy release rate does not fully solve the difficulty of defining the interface strength for continuum interfaces. Numerical calculation of G passes the baton on to fracture components (or to the work of adhesion). Fracture components, or crack-tip loading modes, which refer to an opening, shearing and twisting of the de-adhered ligaments (termed mode I, mode II and mode III, respectively), represent ideal deformations for a crack in a continuum and make way for fracture mechanics, but also they lead to obscured experimental validation.

On the other hand, the failure of adhesion (by specific chemical bonding) at an interface can be understood to require a fixed amount of work. The *work of adhesion* is, theoretically, an accurate quantum mechanics-based concept, but it is difficult to relate a calculation done using quantum mechanics to a micro-scale interface failure—there is a huge range of length scales and structural features separating these two perspectives (Evans, 2006). However, so-called cohesive elements have been formulated for FE; they can be given a zero thickness and addressed to a specific de-cohesion model (sometimes called the 'cohesive zone law'), which defines, consequently, the traction-displacement relationship precisely at the interface. Basically, the use of cohesive elements enables free selection of the de-cohesion model and a variety of parameters, such as those adjusting the viscous dissipation, to be fitted (Cordisco et al., 2012). However, although

being tempting for application-specific problems, the versatility results in cumbersome definitions from the point of view of actual physical phenomena. Not a single generalized, independently consistent de-cohesion model exists.

While being a length scale-free quantity at first glance, the fracture area 'A' in Eq. 2.4 suggests that G might depend on the length scale of the observed failure process. Indeed, the definition of fracture surface is emphasized in the simulations of microscopic systems, where the *apparent* strength on a macro-scale includes effects of small-scale characteristics, such as crack-tip shielding, and, hence, the interface failure separates into something more than a 'clean' crack opening process. In particular, the meaning of an *apparent* measure of strength becomes clear when a crack path is modelled with increasing resolution, i.e. on a length scale beyond the original, selected length scale (Naito and Fujii, 1995; Reedy et al., 2007; Sekulic and Curnier, 2010).

In the following sections, the term 'interface strength' will be used to refer to the mechanical strength of an interface irrespective of the exact definition and measuring technique. The term 'fracture toughness' will be used to refer to the interface strength in terms of either stress intensity factors or energy release rates; no distinction is made due to the overlapping use of these terms in the existing literature as well as in the test standards of the field. Only when the experimental work or simulations presented in this thesis are considered will the precise term be expressed.

2.2.2 Fracture testing

The mechanical failure of multi-component materials is comprised of several physical phenomena and is gradual in time (Ritchie, 2011). When material failure is considered on a micro-scale (or beyond), it initiates at some precise point or local detail rather than occurring throughout the specimen being considered. This is due to geometry-induced stress concentrations, various material imperfections and specific atomic arrangements (Bucknall, 2007; Sen et al., 2010). A stress concentration at the tip of an artificially induced crack or notch is advantageously utilized in fracture testing. In fracture testing, the failure, or, more specifically, crack propagation, is reinterpreted as a fracture toughness value. Practically speaking, fracture testing can be divided into two chronological phases. First, a crack initiates. Second, the crack propagates further in either a stable or an unstable manner. The condition at the time of the crack initi-

ation (of a 'main' crack) is designated a critical condition and it serves as the reference point for *critical fracture toughness* values. Respectively, the stable propagation phase is the reference (point) for *propagation fracture toughness* values.

Pre-crack preparation

For layered multi-component materials, it is important to induce the fracture into the region of interest. That is, the crack-tip must be located in the region of interest so that the observed fracture and the derived fracture toughness values will eventually relate to the critical behaviour of this specific region. In order to control the localization of crack initiation, a pre-crack is prepared onto the fracture test specimens. Consequently, the absolute value of the critical fracture toughness is affected by the pre-crack preparation (Schuecker and Davidson, 2000). Usually, a pre-crack is prepared by laminating a thin, non-adhering polymer film at the intended fracture plane (ISO, 2001). The pre-crack tip can be made sharper by applying a graphite powder or soft lead pencil (Chai, 2003; Sturiale et al., 2007). However, all of these preparations merely create a geometric pre-crack with no plastic region or microscopic crack nucleation, such as a craze deformation (more on this in Section 2.3.2). As a result, the crack nucleation must precede the main crack initiation during the testing.

For the opening mode (i.e. mode I) test methods, it is typical that the test exertion results in a stable crack propagation. For these tests, the crack initiation phase can readily be isolated from the propagation phase—meaning that the exertion can be controlled and released after the crack initiation phase and re-loaded during the propagation phase. Unfortunately, the behaviour of the specimens during those test methods, which leads to a dominant shearing mode (i.e. mode II), tends to be different. For these tests, the crack propagation is often unable to release the strain energy stored in the specimen. The insufficient energy release rate leads to a fast, unstable crack propagation phase. In other words, the critical phase and the propagation phase are difficult to distinguish. Moreover, the pre-crack preparation makes a major contribution to the solitary test output: the critical mode II fracture toughness. The merging of the initiation and the propagation phase and the strong pre-crack dependance make it challenging to determine a correct value—representative of a mode II fracture.

Crack trajectory

Research on crack trajectory focuses on predicting crack paths. Illustrative studies on crack trajectory have been performed by, e.g., Fleck et al. (1991), Chen and Dillard (2001) and Mróz and Mróz (2010). Also, validated criteria for the crack path deflection have been developed, and the generalized effects of material stiffness, the fracture toughness of the bonded materials, residual stresses and mode-mixity have been published in the existing literature. Examples of the criteria include the maximum opening stress criterion (Erdogan and Sih, 1963), the maximum energy release rate criterion (Palaniswamy and Knauss, 1978) and the mode I fracture criterion (Goldstein and Salganik, 1974). In general, the different criteria essentially yield the same results for homogenous (continuum) materials. A continuous mode I loading tends to result in a stable and straight crack path, whereas a mixed mode loading results in crack path deflection. Unfortunately, the criteria are not typically valid for inhomogeneous materials, since the fracture toughness values differ in the vicinity of the interfaces (Chen et al., 2001; Tilbrook et al., 2006).

For a bonded material system, having the crack-tip inside the compliant material, mode II dominance will force the crack to deflect towards the stiffer material (Ryoji et al., 1994; Dillard et al., 1999; Chen et al., 2001). This is a very important result for the testing of metal-polymer interfaces. By using forced mode II crack-tip loading, the crack-tip can be propagated towards and, further, along an interface region, which can be stronger than the compliant layer itself (in terms of fracture toughness). The challenge in generating a mode II dominated crack-tip load during a test is that most of the existing methods, such as the end-notched flexure (ENF) test, tend to press the de-adhered ligaments together; in other words, the frictional effects are unavoidably included (Schuecker and Davidson, 2000; Sun and Davidson, 2005).

Maintaining control of the 'interfacial fracture' during the fracture testing of similar material interfaces, e.g. polymer-polymer interfaces, is clearly more bothersome. The fact that the fracture toughness of the adhering materials as well as of the interface are of the same order vitiates the conscious enforcing of crack deflection—the crack can penetrate through the interface and into either of the bonded materials. Therefore, only a qualitative use of fracture testing applies to realistic (i.e. tough), polymer-polymer interfaces.

2.2.3 Hygrothermal aging

Aging is a term used to describe adverse long-term effects, which result in degradation of the material or interface strength. Hygrothermal aging is assumed to include the effects of absorbed moisture and temperature, in addition to physical aging. Interface regions are especially sensitive to combined aging-moisture effects, and their strength decreases significantly as a result of the diffusion of water molecules (Balkova et al., 2002; Mubashar et al., 2009). It seems that combined aging-moisture effects are inherent to interfaces. The resulting effects on experimentally determined interface strength usually have a stabilizing character, i.e., further degradation does not occur after a certain specimen conditioning time (Loh et al., 2002; Bordes et al., 2009). The moisture can derive from the bonded materials, in addition to the surrounding atmosphere.

The effect of moisture at interfaces, on a molecular scale, is still partly unknown. Most probably, several processes take place and, actually, several concepts have been introduced. The adhesion at metal-polymer interfaces is chiefly based on secondary interatomic forces, i.e. van der Waals forces—only occasionally on chemical (covalent and ionic) bonds. The formation and durability of the bonds highly depends on the preparation of the system, i.e. on the accumulation of residual stresses or contamination (Persson and Tosatti, 2001; Aufray and Roche, 2006). Typical surface treatments increase the surface free energy and, therefore, the substrates are chemically active prior to the bonding procedures. Especially in the event that the bond surface is dominantly polar, it has a tendency to interact with moisture (Evans, 2006). By assuming only secondary interatomic forces, a positive thermodynamic work of adhesion between an oxide surface and a polymer can become negative in the presence of water (Kinloch et al., 2000). The negative work of adhesion can work as the spontaneous driving force of the polar water molecules, which displace the positions of the polymer molecules or functional end groups. Bond loss between polymer molecules and the polar groups of metal substrates has been found to be, at least in part, reversible (Rouw, 1998; Legghe et al., 2009). Moisture can also lower the glass transition temperature, T_g, of the adhering polymer, and the subsequent softening can reduce the toughening via interlocking effects—a low T_g might also increase the adhesive's molecular mobility and, controversially, have an advantageous effect on the interface toughness (Rouw, 1998). In the long run, degrading chemical reac-

tions at the interface (e.g. physical aging and corrosion in the presence of moisture) depend on the precise composition of the system in question (De'Nève et al., 1998; Giunta and Kander, 2002).

Basically, the same fundamentals for the hygrothermal effects of metal-polymer interfaces apply to polymer-polymer interfaces with respect to surface free energy and polarity. Since the system is entirely polymeric, the diffusion of moisture is less restricted and, also, the chemical degradation can make a more significant contribution. In particular, polyesters degrade through hydrolysis reactions in the presence of water (Gu et al., 2001; Partini and Pantani, 2007). The resulting scission of the backbone or dangling chains can promote microscopic processes, such as cavitational damage or osmotic cracking (Bélan et al., 1997).

2.3 Simulation of interface fracture on a micro-scale

2.3.1 Limits of continuum formulation

On a nano-scale, interfaces are typically modelled as systems consisting of individual atoms or molecular entities instead of as a continuum system. These massive calculations are called *molecular dynamics* simulations or *quantum mechanics* simulations and their outputs consists of, for example, adsorption energies or diffusion and friction coefficients between the modelled moieties during motion along a model surface (Drefs et al., 2004; Blomqvist, 2012). A convenient upper limit for a non-continuum simulation size from both the calculation effort and modelled true volume (or length scale) perspective cannot be straightforwardly defined. Nowadays, the question is not whether a discrete material model or a continuum model should be used, but how the two approaches can be combined and which of the length scales work as convenient borders in between the models (Tan, 2002). A neat review of the allocation of different approaches and related length scales has been composed by Jancar (2008); a schematic is shown in Fig. 2.1.

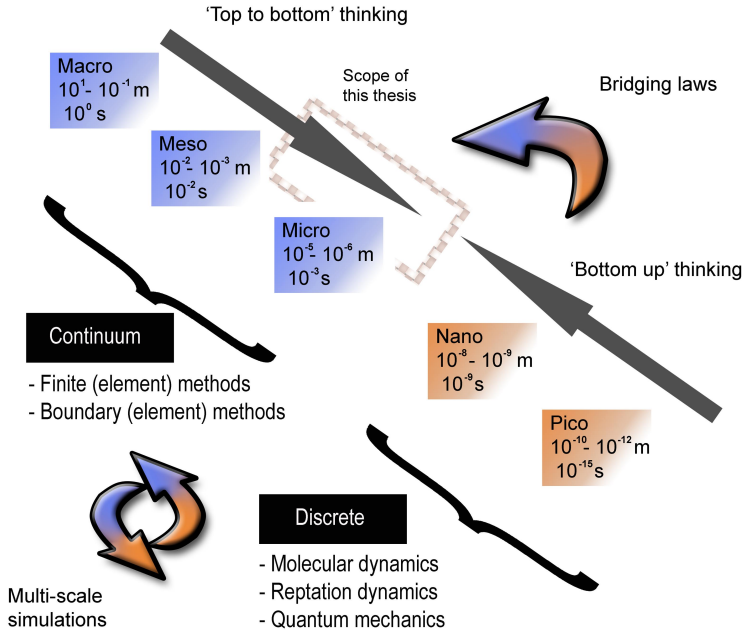

Figure 2.1. Scientific approaches and modelling platforms related to different length scales. Figure reproduced according to a study by Jancar (2008).

Special means are often necessary to unify the gap between the discrete and continuum contexts on a small scale:

1. *Confinement or bridging laws can be used to enhance the physical validity of a length scale-restricted theory.*

2. *Multi-scale simulation can be formulated so that separate, interacting simulations are technically combined to calculate a common problem.*

The latter solution can 'only' help to decrease the simulation efforts and total calculation time—when compared to a single simulation with a comparable resolution. Molecular dynamics simulations and continuum simulations can be merged into a single multi-scale simulation (Jancar, 2008; Johnston and Harmandaris, 2013). For a multi-scale simulation, the models on a smaller length scale are called sub-models. Consequently, the approach to the problem is built from 'top to bottom'.

The former solution means that the theory behind the modelling process is completed by the physics of discrete matter, which derives from a phenomenon on a smaller length scale, that is, the enhancement is

built from the 'bottom up'. An example of a confinement law is the size effect of polymers on strain elasticity, which derives from non-local behaviour of nanoscale inclusions or the long, chain-like molecules in polymers (Sharma and Ganti, 2004; Jancar, 2008). The effect of non-local phenomena covers a *characteristic length scale*, which depends on the material in question (Nikolov et al., 2007). A characteristic length scale can also be seen as an estimate of the lower bound of a self-standing, continuum mechanics-based simulation. The characteristic length scale for metals is of the order of the lattice parameter—approximately 0.25 nm (Zhang and Sharma, 2005). For graphite, a length scale of approximately 3.3 nm has been reported (Reid and Gooding, 1992). The characteristic length scale for polymers strongly depends on the type of polymer because the molecular interactions are significant and the deformations are highly heterogeneous and also because there are excluded-volume effects; observations on a nano-scale indicate characteristic length scales of several nanometers (Wübbenhorst and Lupascu, 2005).

2.3.2 Challenge of gradual fracture

Continuum simulations of plasticity at interfaces

A crack-tip, on a sub-micron scale, experiences yielding with most materials. This is a challenge for continuum simulations, which rely on the assumption of a sharp crack-tip and which allow only for a single crack in the vicinity of the (main) crack-tip (Elices et al., 2002). Many studies have wound around the effects of yielding and plasticity by exploiting the concept of a crack-tip embedded in brittle, linear material *surrounded* by a yielding material (Sugimura et al., 1995; Tilbrook et al., 2005). The effect of an elastic-plastic layer near the crack-tip in a bi-material is twofold. In the event of a crack-tip inside a compliant layer, such as a polymeric interphase, an adjacent stiff layer (e.g. metallic substrate) would offer elastic shielding (see Section 2.1.1) followed by a toughening effect (Fleck et al., 1991). Second, a more ductile layer (i.e. lower yield strength) just above the layer with a crack can toughen the interface region due to the energy dissipation of plastic deformation (Sugimura et al., 1995; Tilbrook et al., 2005). The dissipated energy and the toughening are proportional to the extent (thickness) of the ductile layer, but eventually they will diminish due to an anti-shielding effect of the thick ductile (and compliant) layer.

Cohesive elements allow for yielding and plasticity in the immediate vicinity of a crack-tip. The technical challenge has to do with the deformation of the element mesh due to plastic strain. Simulations that allow for plastic deformation at a crack-tip are prone to fail due to extensive mesh distortion (Zavattieri et al., 2008). The mesh distortion, in theory, could be solved by using adaptive meshing (Trädegård et al., 1998; Bouchard et al., 2003). However, adaptive meshing has not been greatly utilized for interface simulations, and it would require placing a great deal of emphasis on the mesh-dependence. To give an idea of the amount of deformation in polymers, the draw ratio of craze fibrils in front of a crack-tip can be in the order of five until the blunted tip opens into a crack (Bucknall, 2007).

Continuum simulations of structural flaws

Studies on flaws at interfaces and their related influence on continuum fracture date back to the year 1965, when Erdogan (1965) formulated general, analytical solutions for the stress fields at idealized, elastic interfaces. The next step in the simulation of flaws at interfaces was taken when boundary element methods and finite element methods were adopted within the field of science. Mammoli et al. (1995) used the boundary element method to simulate crack propagation through (i.e. perpendicular to) an ideal, elastic interface containing a finite de-bond. They reported that the de-bond caused the crack-tip loading mode-mixity (of the propagating crack) to shift and increased the likelihood of crack deflection; the cracks tended to be attracted towards flaws.

In practice, a structural flaw can result due to a human-induced error during the specimen preparation. Cheuk and Tong (2002) used the finite element method to simulate a two-dimensional, millimetre-scale delamination embedded in a composite adherent laminate. They studied the effect of a finite delamination on the apparent shear strength of adhesively bonded, single-lap shear specimens; their conclusions state that the delamination inside the adherent caused a significant reduction in the apparent failure load (of the joint). Feraren and Jensen (2004) simulated the effect of circular de-bonds along the path of delamination in an adhesive joint. They modelled the interface (adhesive layer) using cohesive elements and three different sets of material parameters; their conclusions state that the apparent joint strength was affected only when the crack front propagated in the vicinity of the de-bond.

Continuum simulations of crazes and dislocations

For metallic materials, the formation of new crack surfaces is greatly affected by the metal's grain structure (Traiviratana et al., 2008). In addition to the grain-specific properties, the grain structure controls the dislocation movement and the individual grains can separate or slide in relation to one another (Qi and Krajewski, 2007). O'Day et al. (2006) used a combined discrete-continuum method for a bi-material simulation and studied the effect of the accumulation of dislocations in the substrate on the interface fracture. Their interface, modelled between a fully elastic coating layer and a plastic (discrete dislocations) metal substrate, was modelled using a typical traction-separation cohesive law. They reported that the delamination of the coating layer from the metal substrate could be divided into two totally separate processes on a micro-scale; the progression of the crack was an energy-driven process and the nucleation of the crack-tip was a stress-driven process—being directly dependent on the accumulation of dislocations.

On a sub-micron scale, the formation of new crack surfaces in polymeric materials is preceded by molecular re-orientation (e.g., shear banding of the molecular network), cavitation (of rubbery phases), void escalation and craze formation. Crazes are specific molecular-scale formations created by fibrils of densely orientated polymer chains and free volume. Craze fibrils can be tens of nanometres long and the distance to the next fibril a few micrometres. Both the initiation and deformation of a craze fibril are highly visco-elastic processes and they depend on the strain rate as well as the temperature during the elongation. It should be noted that actual cracks can form without any craze initiation and that specific flaws, such as spherical voids or bubbles, do not inevitably lead to craze initiation—yet this necessitates specific circumstances. Basu et al. (2005) simulated a craze fibril deformation using the finite element method. Although they presumed a continuum formulation, they still needed to account for discrete behaviour, which in reality derives from the three-dimensional, entangled network of chains and related 'locking' and 'strand slip' mechanisms. Their results called attention to the formation of 'active zones' due to local softening of the polymer and verified a relationship between network entanglement and the fibril geometry.

3. Methods and conducted work

3.1 Methods

The research work done in the thesis consisted of both experimental work and numerical simulation. The applied methods are introduced in the following. The reader is kindly asked to turn to the related publications (Publications I–VI) for more details of the methods.

3.1.1 Single-lap shear test

Single-lap shear testing is probably the most popular test method for evaluating the strength of adhesive joints. The determined measure of strength is the average shear strength calculated based on the fracture area and peak load at failure. In addition, the fracture surfaces and the load response during the loading can be studied in order to obtain more information about, for example, the fracture locus or work of fracture. It should be noted that the adhesive thickness, load rate, adherent bending due to the excentric load path and the edges of the overlap region (where fillets might form, see Fig. 3.1) significantly affect the specimen's internal stresses and, consequently, the determined strength values (Tsai and Morton, 1995). Moreover, the determined shear strength does not relate to the behaviour of the interface at all in the event that the failure occurs inside an adherent (or adhesive, if used). In Publication VI, single-lap shear testing was applied based on the ASTM D5868 standard.

3.1.2 Wedge test

A wedge test is a fracture test method for studying the durability of adhesively bonded joints. The wedge specimen is a beam consisting of two

bonded adherents and a pre-crack prepared at the other end. The specimen is loaded (fractured) by inserting a metallic wedge (see Fig. 3.1) and the crack propagation is monitored as a function of time. During the crack propagation, the specimen is immersed in a conditioning medium, e.g. water. The wedge insertion creates relatively pure mode I crack-tip loading. In Publication VI, the wedge testing was applied to composite-composite joints to study the effect of surface treatments and water immersion on interface strength; a standard procedure exists only for metallic adherents (ASTM D3762). The mode I energy release rate for the crack tip can be estimated using the following equation (Brown and Pilla, 1982):

$$G_I = \frac{Y^2 E t^3 \left[3(a + 0.6\,t)^2 + t^2\right]}{16\left[(a + 0.6\,t)^3 + a t^2\right]^2}, \tag{3.1}$$

where Y is the crack opening displacement, E is the Young's modulus of the adherents, t is the adherent thickness and a is the crack length.

3.1.3 Double cantilever beam test (DCB)

A double cantilever beam test is a fracture test method for studying the fracture resistance under pure mode I crack-tip loading. The specimen is a beam consisting of two bonded adherents and a pre-crack prepared at the bond line. The specimen is loaded at load blocks (or hinges) fixed to the adherents so that the adherents bend creating an opening displacement at the crack-tip (see Fig. 3.1). Standard procedures exist for metallic (ASTM D3433) and composite adherents (ASTM D5528 and ISO 15024). The standard procedures give guidance for determining both the initiation and propagation-related fracture toughness values. In Publication VI, DCB testing was used to study the effect of surface treatments and moisture absorption on interface strength. The mode I energy release rate can be calculated as follows (ISO, 2001):

$$G_I = \frac{3L\delta}{(2b\left[a + \Delta\right])} \cdot \frac{F}{N}, \tag{3.2}$$

where L is the load, δ is the displacement at the load line, b is the specimen width, a is the (momentary) crack length, Δ is the crack length correction term, F is the large-displacement correction factor and N is the load block correction factor. During testing, manual marks are given to synchronize the momentary location of the crack-tip and load–displacement data.

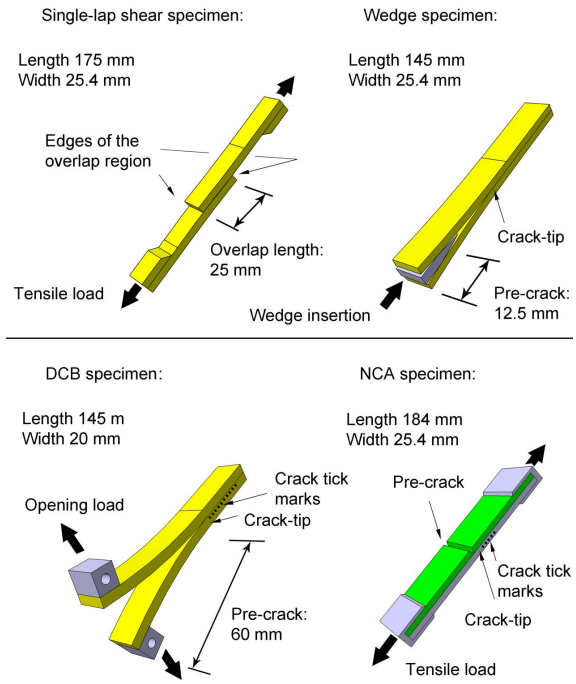

Figure 3.1. Schematic illustration of the specimens used for the single-lap shear test, wedge test, DCB test and NCA test. The specimens are not drawn in scale.

3.1.4 Notched coating adhesion test (NCA)

Notched coating adhesion test (NCA) is a fracture test method for studying the strength of an interface between a coating and a clearly stiffer substrate (Fig. 3.1). The determined measure of strength is fracture toughness and its value is calculated based on the substrate strain at the time of the crack onset. For typical pre-crack preparation techniques, the crack onset leads to an immediate collapse of the interface throughout the entire specimen. An NCA test cannot be used to produce either pure mode I fracture toughness (G_I) or mode II fracture toughness (G_{II}) values. The exact mode-mixity value ($\psi = \text{atan}(G_{II}/G_I)$) can be analytically estimated and, its value varies between $\psi \approx 40^\circ$ and $\psi \approx 70^\circ$ for typical metal-polymer bi-materials (Suo and Hutchinson, 1990; Dillard et al., 1999). This means that the NCA method is capable of generating mode II *dominated* crack-tip loading. In publication II, an NCA test was applied to studies of the interface strength between a stainless steel substrate and an epoxy coatings. The deformation in the specimens was measured using an extensometer (MTS, USA) and strain gages (Kyowa, Japan). An optical microscope was used to observe the crack propagation and synchronized marks

were given for every two-millimetre-long crack advancement. The way in which the critical energy release rate values were determined using the NCA test data will be discussed later in more detail (Section 3.2.4).

3.1.5 Profilometry

Profilometry refers to either laser diffraction or stylus scanning in order to determine geometric surface shapes. It is important to notice that a stylus profilometer is able to measure shapes with a 'characteristic' size that is less than the tip radius of the stylus being used. Also, the operator-adjusted stylus force (to track the surface) can be too high and, annoyingly, damage the finest shapes. In the work presented in Publications I and II, a stylus profilometer was used for specimen curvature measurements (*Dektak 6M*, Veeco Instruments, USA).

3.1.6 Acoustic emission measurement (AE)

Acoustic waves are a form of failure energy; part of the strain energy stored in a (mechanically) loaded specimen is transformed into acoustic emission during fracture. AE is typically arranged at the same time that destructive testing is done. The emission spectrum observed during the loading and, ultimately, during the failure of the test specimen can provide information about a variety of micro-, meso- and macro-failure processes (Andreikiv et al., 2001; Skal's'kyi et al., 2003). Decomposition of the emission data is typically needed; for example, the accumulation of signal peaks or frequency profiles can be determined (Qi et al., 1997; Sause et al., 2012). Also, efficient background noise suppression and adjusted thresholds are necessary in order to distinguish between relevant emission bursts. Moreover, it is important to consider the proper path of acoustic waves from the emission source (i.e. the failure process zone) to a detector, the type of detector being used, electrical noise and the noise generated by the testing machine. In Publication III, a tailored system was applied. The system was based on a 150 kHz, *VS 150-MS* detector (Vallen, Germany) and an integrated *ACU 100* analyser unit (Andritz, Finland). The system was capable of fast Fourier transform (FFT) frequency analysis and also adjustable, event-based amplitude detection.

3.1.7 Differential scanning calorimetry (DSC)

Differential scanning calorimetry (DSC) is used to determine the heat consumed by the molecular transformation and the chemical reactions in a polymer sample. During a typical measurement, a constant-slope temperature ramp is subjected to the sample. First, the DSC data, i.e. the heating rate profiles, can be analysed to determine the heat of cure (polymerization) or crystallization related to an exothermic (endothermic) peak in the profile and also the glass transition temperature (T_g) of a polymer sample. T_g is always measured for a fully cured sample in case repeated heating runs might be needed. It should be noted that the momentary heat can also be negative, meaning that the sample has been cooled down due to exothermic reactions (and to preserve the adjusted temperature ramp). In Publication VI, DSC was used to study the degree of cure during the formation of polymer-polymer interfaces related to tear ply pre-treatments. The instrument used was the *DSC 204 F1* (Netzsch, Germany).

3.1.8 X-ray diffraction surface stress measurement (XRD)

The X-ray diffraction surface stress measurement (XRD) method is based on the diffraction of X-rays. The X-ray diffraction pattern is governed by the nuclei in the atomic lattice structure of a metallic sample. A measured diffraction (solid) angle of the X-ray beam can be directly related to the interatomic distances and compared to a reference data of an 'unstrained' (no external loading) sample to derive the (continuum) stress state of the strained sample. Since the X-ray diffraction escapes the sample surface at approximately a depth of a few microns, the derived stress state is called the surface stress state. A basic plane-stress state or, alternatively, a full three-dimensional formulation can be achieved when calculating of stress components in a Cartesian coordinate system.

The unstrained reference state often includes residual stresses resulting from the manufacture of a specific sample material. Consequently, the change in the stress state due to external loading can be affected by the sample's unstrained residual stress state as well as by its microstructure. In addition, the scattering process is affected by the surface condition, meaning cleanliness and surface oxide formations. The instrument used for the work presented in Publication I was the *Xstress 3000 G1 (G3)* (Stresstech Group, Finland).

3.1.9 Field-emission scanning electron microscopy (FESEM)

Scanning electron microscopy is a powerful method used to reveal detailed surface morphology. On a sub-micron scale, however, it is required to account for differences in electron penetration and induced electron emittance for media with different elemental content. On the other hand, the elemental distributions-induced variation in the imaging contrast can be used to gain additional (although qualitative) information about the sample surface. Selective imaging of differently scattered electrons is also possible by selecting the detector that should be used. In practice, low acceleration voltages are necessary for polymeric samples due to the predominance of light, low-z (atomic number) elements. Also, because polymers have an insulating nature, a compromise must be found between a minimum surface coating and adequate imaging quality at the required resolution. This note also applies to metallic samples when low-z elements containing formations (e.g. oxides) on the surface are studied at a very high magnification. The electron microscopy presented in Publications II–VI was conducted using the *ULTRAplus* (Zeiss, Germany) and most of the imaging was conducted using a secondary electron detector. The instrument's electron gun is a field-emission source that produces a beam with a high degree of brightness, a low energy spread and a small spot size when compared to Lab6 and tungsten sources. Therefore, the instrument is termed a field-emission scanning electron microscope.

3.1.10 X-ray energy dispersive spectroscopy (EDS)

When scanning a surface uisng an electron beam, the electron cloud of the atoms in the sample interacts with the electrons from the beam. When the beam-activated state of an atom's inner-shell electron decays, it can emit an X-ray with a characteristic energy level. These energy levels can be associated with elemental codes. The occurrence of characteristic X-rays is element-dependent, as is their detection; X-ray energy dispersive spectroscopy (EDS) is clearly less sensitive to low-z elements. The characteristic X-rays, induced via the electron beam can escape the sample material at a depth of approximately one micron—this represents the sampling depth of the method. Specifically, the collected data at a certain point represents the integral average of the (surface) composition enclosed by a spherical volume with a diameter of approximately 1 µm. Technically, the X-ray spectrum is recorded using a specific detector installed on an

electron microscope. In Publications III and VI, the *INCAx-act* (Oxford Instruments, UK) was used; it was installed on the FESEM instrument described above.

3.1.11 X-ray photoelectron spectroscopy (XPS)

X-ray photoelectron spectroscopy (XPS) can be used to detect and analyse the electrons emitted from the sample surface by a photon energy from an X-ray source. In general, XPS refers to photoelectron spectroscopy (PES) in which the photon energy is in the range of 100 eV–10 keV. The XPS sampling depth, meaning the range of depth involved with the photoelectron process, depends on the wave length of the source X-rays, the detection angle and elemental content of the sample surface (i.e. the material's work function). In general, the sampling depth for the most of materials is in the range of 3–15 nm. The sensitivity of the technique is at a reliable level for elements ranging from lithium to uranium, and quantitative data on the electron states (core level) can be achieved under ultra high vacuum conditions. The XPS study presented in Publication III was performed using the *AXIS 165* (Kratos Analytical, UK). More details on this particular instrumentation and vacuum setup can be found in a study by Johansson (2002).

3.1.12 Atomic force microscopy (AFM)

Atomic force microscopy (AFM) is a versatile microscopic measurement method for studying surfaces ranging from a sub-micron scale to an atomic scale. The probe of an atomic force microscope is typically a pyramidal silicon tip and the tip is attached to a metallic, cantilevered beam. Typical measurement output, i.e., the height data, basically consists of the feedback signal adjusting the tip at a 'constant' distance from a sample surface during scanning. The displacements from the cantilevered beam's head, where the tip is attached, are determined using a laser reflected from the beam head, as illustrated in Fig. 3.2. The beam head experiences a deviation whenever a local detail on the sample surface interacts with the silicon tip. The sample surface can interact with the tip via mechanical contact forces, van der Waals forces, capillary forces, electrostatic forces, chemical bonding, magnetic forces, Casimir forces and solvation forces. An oscillatory measuring mode, namely a tapping mode, was applied for the measurements presented in Publications III and IV. This means that

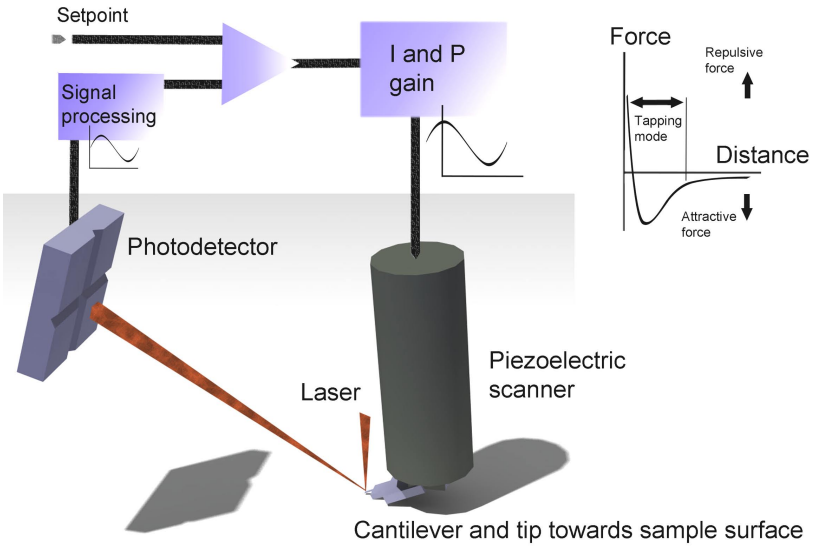

Figure 3.2. Schematic of the working principle of an atomic force microscope. During operation, the microscope is controlled by adjusting several parameters, e.g. the amplitude setpoint and the integral (I) and proportional (P) gains. The inset force-distance graph shows the sample surface-tip interaction zone of the tapping mode.

the cantilever head is forced into a controlled vibration during the scanning process; usually a sinusoidal motion at a cantilever's natural frequency is used. For the tapping mode, the tip motion is to remain in a zone where the surface attractive forces turn into repulsive forces. That is to say, the tip is not supposed to encounter mechanical contact forces (from the sample surface). The tapping mode also makes it possible to measure the time-lag between an observed deviation from the cantilever's motion and the adjusted control signal, i.e. dissipated cantilever's kinetic energy, which is recorded in the form of so-called phase-difference data. Due to the multiple surface forces involved, the phase-difference data are only able to indicate a change on the sample surface that can be related to a compositional deviation (but not to a morphological change alone). For the studies presented in Publications III and IV, an integrated, main unit-controller system, the *Dimension 5000 – Nanoscope 5* (Veeco Instruments, USA), was used. The nominal tip radius was 10 nm and its quality was verified using a calibration sample. A computer software (*Gwyddion*, version 2.25) was used for data post processing and image generation.

3.1.13 Analytical residual stress estimation

An analytical stress-deformation model was used in the studies on bi-material residual stresses. A two-dimensional model, originally presented by Yu et al. (2006), was applied and also validated for the specific metal-polymer specimens studied in Publications I–III. The model is based on the assumption of an ideal (fixed) bond and linear thermal expansion and it can be used to calculate thermal residual stresses as a function of the specimen's thickness coordinate. Experimental data on the bending (e.g. radius) of a bi-material specimen can be implemented for the calculation; then, the model can be used to solve for one of the material constants. The model presumes linear elasticity and the simplified cross-sectional deformation from the classical beam-bending theory.

3.1.14 Finite element analysis (FE)

The finite element method applied in the fracture study presented in Publication IV refers to a commercially available computer code, *Abaqus*® (Dassault Systèmes, USA). This code can be used to numerically simulate and calculate a diverse range of both solid state and flowing matter problems. The code includes blocks for modelling the geometry, interactions and external and internal loads of the problem in question, in addition to the blocks for finite element meshing and the actual problem solver. Solving the modelled problem involves a numerical iteration and, thus, the solution is in part dependent on the given control parameters and actual iteration algorithm of the code's solver block. The convergence of the iteration is partly dependent on several independent and interdependent (adjustment) parameters, which are determined by the operator.

3.1.15 Virtual crack closure technique (VCCT)

VCCT is a numerical method that can be implemented for an FE code to calculate the energy release rates when a propagating crack is simulated. The fundamental background to the method is linear fracture mechanics and, in particular, a linear force-displacement relationship at the crack-tip. The crack-tip loading modes are used in managing the steep deformation gradients at the crack-tip; the opening, shearing and tearing fracture modes are considered. VCCT requires implementing a fracture criterion for the crack propagation, i.e. for opening the finite element nodal contact;

experimental material parameters are needed for the fracture criterion. In Publication IV, a power-law criterion was used. A comprehensive description of VCCT has been provided, for example, by Krueger (2004).

3.2 Interface strength at a metal-polymer interface: Work conducted in Publications I–III

3.2.1 Surface condition of AISI 304 based on the existing literature

Micro-scale surface morphology

Stainless steel alloys in general have proved to bee challenging substrate materials for structural applications that require bonding using a polymeric adhesive (Van Rooijen et al., 2005). The effect of the stainless steel's surface oxide composition and its structure has not been studied relative to the adhering polymer's chemical reactions, but the results from different etching and electrolytic surface treatments used for adhesive bonding provide some evidence that grooved grain boundaries could enhance the adhesion at the metal-polymer interface (Bouquet et al., 1992).

The dissolution of austenitic stainless steel during an *electropolishing* treatment involves anodic surface levelling and anodic brightening, both which tend to level surface morphology on a micro-scale. Anodic levelling is related to different dissolution rates at peaks and valleys on the surface, whereas anodic brightening in turn is related to suppression of the effect of steel microstructure on the dissolution rate (Lin et al., 2009). These electropolishing phenomena require a certain amount of phosphoric acid (H_3PO_4) in the electrolyte medium or otherwise iron passivity will hinder the mass transport (Ponto et al., 1987). Typically, aqueous mixtures ($\approx$15% water) of sulfuric acid (H_2SO) and H_3PO_4 are used.

Phosphoric acids are weak acids in general and, hence, a phosphoric acid immersion alone does not have a significant effect on austenitic stainless steel in terms of metal dissolution. Phosphoric acid mediums at high temperatures (> 100 °C) and at very high phosphoric acid concentrations (98%) have been observed to result in some iron-oxide enrichment and diffused phosphorus at the topmost oxide layer (Wang and Turner, 2008). In contrast to phosphoric acid solutions, strong nitric acid (HNO_3) solutions are capable of chemical dissolution of austenitic stainless steel dur-

ing pure immersion (termed *etching*). The maximum dissolution rate can be found by adjusting the immersion medium's temperature and HNO_3 concentration (Kolman et al., 1997). Depending on the etching parameters and precise stainless steel alloying, nitric acid etching tends to result in highly fragmented surfaces due to the increased dissolution at surface inhomogeneities, such as the grain boundaries (Beckit et al., 1988).

Oxide layer structure and composition

Austenitic stainless steels form a chromium-enriched oxide layer on their free surfaces when exposed to oxygen in the air. The oxides work as a barrier against further oxidative reactions and enable efficient corrosion resistance. The oxide layer in total is extremely thin—its thickness ranges from approximately 0.5 to 20 nm (Lothongkum et al., 2003; Honkanen et al., 2011). The oxide layer has an internal structure that is composed of a chromium-hydroxide coverage and anhydrous chromium-oxide intermediate layer against the bulk steel (Köver et al., 1983). In more detail, the lower, chromium-oxide layer has been observed to involve an upper layer with some iron oxide and a sub-layer consisting of only chromium oxides facing the bulk steel. All of the layers containing chromium oxide also include residues of chromium, iron and nickel, depending on the precise alloying of the steel in question (Lothongkum et al., 2003).

Different surface treatments can modify the stainless steel's native oxide layer structure. Acidic immersion mediums tend to result in a topmost layer that is pure chromium hydroxide, whereas alkaline mediums can lead to the occurrence of some iron oxides in addition to the prevailing chromium hydroxide (Maurice et al., 1996; Abreu et al., 2004). Nitric acid and sulfuric acid immersions have been reported to decrease the overall metal oxy-hydroxide content and increase the metal oxide content of the surface (Lothongkum et al., 1999). Neutral clean water immersion (pH ≈ 7) and heating in air at low temperatures (< 250 °C) have not been observed to affect the layered structure or compositional distribution of the surface (Köver et al., 1983).

3.2.2 Control of the substrate surface condition for the thesis experiments

Since studies on adhesive bonds with stainless steel substrates are scarce in the existing literature, Publications I–III aimed to study experimentally the interface strength between stainless steel and epoxy. A commer-

cial film adhesive was chosen to avoid hands-on resin mixing and also to ensure strong, practical bonds. The main focus was to describe the share of surface morphology in interface strength. For this, three different substrate series with three different surface conditions were acquired. The substrate surface pre-treatment procedures for controlling the morphology are shown in Table 3.1. After the pre-treatments, a cleaning procedure was applied to ensure cleanliness prior to the adhesive application. The cleaning procedure applied to the stainless steel substrates after the pre-treatments is shown in Table 3.2. The fourth cleaning process phase involved a gentle etching using a phosphoric acid based immersion medium and its function was to remove oxide-based impurities and also to introduce compositional similarity into the outermost oxide surface.

Table 3.1. Three different surface pre-treatments for AISI 304 stainless steel substrates (Publications I–III)

Surface condition	Immersion medium (v/v)	Current density (A/dm^2)	Temperature (°C)	Duration (min)
As-received	-	-	-	-
Etched	HF 3%, HNO_3 20%, H_2O 77%	-	18	720
Electropolished	H_2SO, H_3PO_4, H_2O (mixture)	≈ 215	30	5

After the cleaning procedure, each substrate condition was analysed relative to the surface cleanliness and morphology; any possible variation in the oxide scale was beyond the length scale of the study. A typical cleaned surface of an as-received substrate is shown in Fig. 3.3; the figure shows the deep grooves that surround each grain on the stainless steel substrate. The grains varied in their diameter over a range of approximately 5 µm to 25 µm. Extracted values from the AFM height data, as illustrated in Fig. 3.3, revealed that the grooves were approximately 1 µm wide and 1–2 µm deep. When compared to the as-received substrate condition, the FESEM imaging and AFM measurements showed that the etching pre-treatment not only removed material at the grain boundaries but also created sharp ridges on the individual grains. The electropolished substrate surfaces were clean and essentially flat on a sub-micron scale (see Fig. 3.3).

Table 3.2. The cleaning process developed for surface-treated AISI 304 stainless steel substrates prior to adhesive bonding (Publications I–III)

Treatment	Action	Medium	Temperature	Duration
Degrease	Wiping	Acetone	RT	-
Micro-pore cleaning	Sonicating bath	Tap water	50 °C	6 min
Rinsing	Immersion	Distilled water	RT	5 min
Oxide impurities cleaning	Immersion	Distilled water, phosphoric acid based solution (10 % v/v, pH ≈1.8)	63 °C	10 min
Rinsing	Immersion	Distilled water	RT	5 min
Dehydration	Vacuum oven	Air, 0.9 bar vacuum	71 °C	55 min

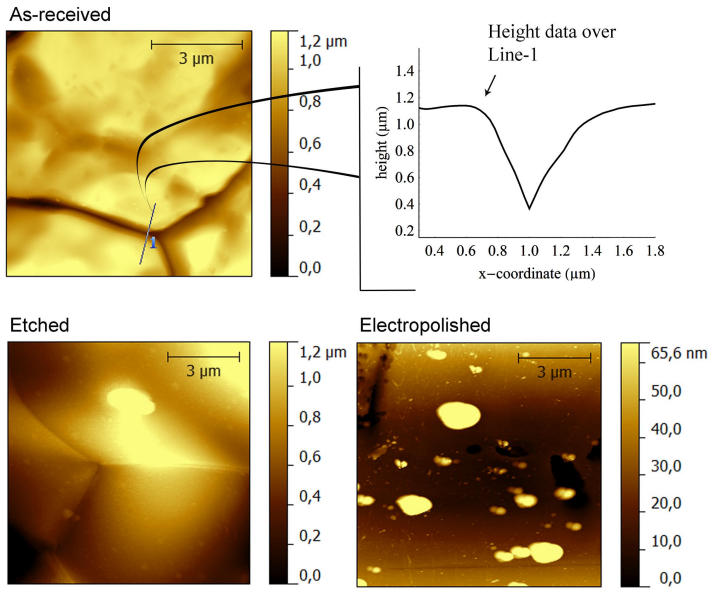

Figure 3.3. AFM height data measured on different stainless steel substrates after cleaning. Data on the as-received surface show deep grain boundary grooves between the grains; extracted data across the grain boundary groove show that the local width is ≈1 µm and the depth ≈0.8 µm.

3.2.3 Residual stresses at bi-material interfaces

Due to the bonding that takes place at an elevated temperature, residual stresses in metal-polymer bi-materials have been studied in the existing literature (e.g. Timoshenko, 1925; Sanderson, 2008) but the existing models have not been validated in the vicinity of interfaces. Publication I aimed to study thermal residual stresses at an interface between the stainless steel substrate and epoxy. Analytical estimates were calculated using a method introduced by Yu et al. (2006). True stresses and the deformation of bonded specimens were studied using XRD and profilometry, respectively. Longitudinal stress components were calculated based on the XRD data (principal stresses) using the plane-stress state transformation law (see, e.g. Parnes, 2001). The results indicated that the analytically estimated stress distributions at the interface corresponded to the experimental results. Due to the XRD's sensitivity to the substrate's surface condition, three different surface conditions were studied (shown in Table 3.1). The study reported that the electropolishing treatment lowered the scatter of XRD results. All three specimen series arrived at a rather similar residual stress state, but there was considerable variation in the deformation shape for all three specimen series.

3.2.4 Fracture test method development

Publication II aimed to produce interface fracture toughness values as accurately as possible. The study concentrated on minimizing the variation in the experimental data and also described the factors affecting the variation. The means for minimizing the variation were as follows:

- Hands-on specimen preparations were kept at minimum and particular attention was paid to substrate cleaning prior to bonding.
- Residual stresses were accounted for on a specimen-by-specimen basis.
- Pre-crack preparation was performed systematically.
- Critical energy release rate was determined using strain-rate profiles.

The specimen preparation process was designed to minimize the hands-on work phases and improve substrate cleanliness, as discussed in Sec-

tion 3.2.2, and the developed cleaning procedure (see Table 3.2) was applied to all of the specimens studied in Publications I–III. The following subsections will discuss the other three items listed.

Energy release due to residual strain

The notched coating adhesion (NCA) fracture test method has been analysed by Dillard et al. (1999). According to the analysis, the elastic strain energy release can be calculated by assuming that the delaminating layer has a finite width and thickness and also that bi-axial residual strains contribute to the strain state. Hence, the strain energy release rate at the time of the interface collapse, G_c, can be calculated as follows:

$$G_c = \frac{hE}{(1-\nu)}\left[\varepsilon_0^2 + \varepsilon_0\varepsilon(1-\nu_s) + \frac{\varepsilon^2(1-2\nu\nu_s+\nu_s^2)}{2(1+\nu)}\right], \tag{3.3}$$

where h is the thickness of the delaminating layer, ε_0 is the bi-axial residual strain in the delaminating layer, ε is the critical longitudinal mechanically induced strain, E is the Young's modulus of the polymer (the delaminating layer) and ν and ν_s are Poisson's ratios of the polymer and substrate, respectively. The critical longitudinal strain refers to the value of the test-induced strain at the time of interface collapse. In Publication II, the bi-axial residual strain, ε_0, was estimated by measuring the curvature in each tested specimen using a profilometer and by calculating the uniaxial residual stress according to the procedure described in Publication I. Furthermore, Hooke's law was presumed when converting the bi-axial residual stress into strain:

$$\varepsilon_0 = \frac{(1-\nu)\sigma_0}{E}. \tag{3.4}$$

In Equation 3.4, the bi-axial residual stress, σ_0, was assumed to correspond to the uniaxial, analytical estimate. Additionally, the effect of the straightening of a curved specimen during the testing was taken into account in the induced strain state (ε), although the influence on the interface fracture toughness values was found to be minor.

Systematic pre-crack preparation

Prior to conducting an NCA test, a pre-crack must be prepared, i.e. a cut must be made through the polymer layer. Dillard et al. (1999) suggested using a surgeon's knife. However, manual cutting is prone to operator-dependent, faulty pre-cracks. As a solution to the pre-crack preparation problem, Publication II introduced a systematic pre-crack preparation technique. A pre-crack device was developed and it was designed to be

used together with a servo-hydraulic testing machine. The idea is that the force-controlled load subjected to a wedge in the device results in precise cutting over the entire width of a specimen. Each pre-crack was prepared in two steps:

1. A steel wedge was use to cut through the polymer layer.

2. Using an aluminium or copper wedge, the polymer layer in the neighbourhood of the cut was loaded to extend the pre-crack along the interface in a controlled manner.

Eventually, the length of the pre-crack along the interface must be long enough compared to the thickness of the polymer layer (Dillard et al., 1999), i.e., Equation 3.3 assumes that the lateral constraint of the specimen does not prevent free lateral expansion of the delaminating layer due to Poisson's effect. In practice, the peak load for the cut and extension step, as well as suitable wedge material, can be found via a few trial runs.

In publication II, it was observed that the systematic pre-crack preparation resulted in a three-phased crack propagation (instead of an instant, unstable collapse). During the testing, it was not possible to observe the crack initiation by the operator using an optical microscope because the opening of the crack-tip was small and the plastic zone unobservable. Besides, the strain-rate profiles indicated crack initiation before the first manual mark. Therefore, initiation on a micro-scale was studied by comparing the power released by the crack-tip during the stable propagation phase, P_{avg}:

$$P_{avg} = G_c v_t, \tag{3.5}$$

where G_c is the critical energy release rate based on the critical substrate strain and v_t is the crack-tip velocity from the stable propagation phase until the final interface collapse. The product with fracture toughness signifies direct dependency on the test machine's load rate. The behaviour of polymeric materials at bi-material interfaces is strain-rate dependent (e.g., Gent and Schultz, 1972) and hence it is natural that the crack initiation would depend on the load rate. In other words, the load rate selected for the NCA testing (1 mm min^{-1} in Publication II) could affect the initiation order (between specimen configurations).

The sensitivity of the pre-crack preparation to interface fracture toughness was studied in Publication II by analysing the inverse of the pre-

crack length as a function of the specimen's storage time. It was noted that the plotted values expressed the same aging behaviour as the G_c values (using Equation 3.3). Therefore, it was shown that the systemically prepared pre-cracks were governed by the material failure at the correct crack locus and as well as by the related critical energy release rate value of the interface.

Definition of interface collapse

During the work reported in Publication II, it was noted that visual observations of the interface collapse were highly inaccurate; it was very difficult to observe the collapse due to the small crack opening and negligible plastic zone. Therefore, the strain distributions in the specimens were studied in more detail. It was noted that local bending and also spring-back occurred due to the change in the specimen's stiffness at the time of crack onset. These phenomena were observable from the NCA test data, as illustrated in Fig. 3.4. Two uniaxial strain gages per specimen were fixed to the steel substrate's back side prior to testing.

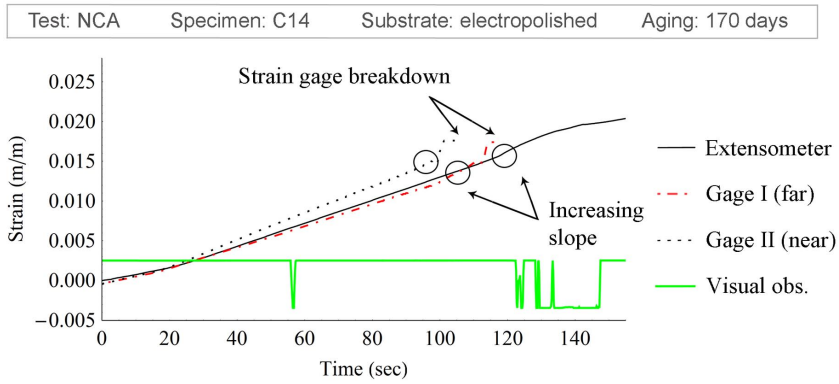

Figure 3.4. Measured strains during the NCA fracture test. Increasing slope indicated the crack propagation along the interface, which first reached the strain gage near the pre-crack tip and then the strain gage far from the pre-crack and, finally, the entire specimen (the extensometer data). The displacement transducer signal of synchronized manual marks based on the visual observation of crack initiation and propagation is plotted as well.

To emphasize the different phases in the specimen's behaviour, strain-rate profiles were analysed. Based on the simultaneous visually observed crack growth and respective marks, three distinguishable phases of interface fracture were defined, as illustrated in Fig. 3.5. Henceforth, the peak of the strain rate profile was used as the definition for the critical strain value (see Equation 3.3) of each tested NCA specimen.

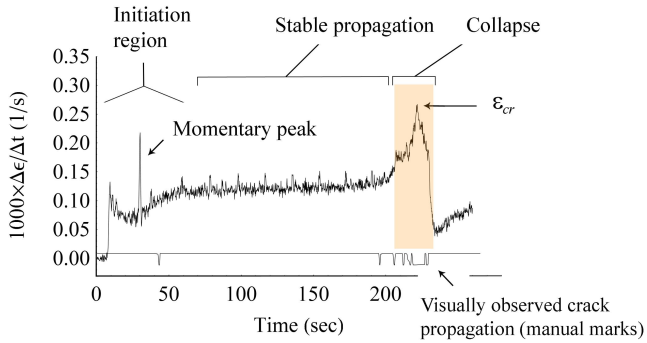

Figure 3.5. A typical strain-rate profile showing the three phases of crack propagation during an NCA fracture test; only the stable propagation phase and the collapse were observable from the measurement data. The critical strain, ε_{cr}, was defined as the strain at the maximum peak in the strain-rate profile during the collapse phase.

3.2.5 Variation in critical energy release rate values

In Publication II, the contribution of the substrate morphology and storage time (aging) were studied to describe the related effects on the variation in the critical energy release rate values. The values obtained as a result of the NCA fracture testing are shown in Table 3.3. Initial estimates of the share of substrate morphology can be made by assuming that the electropolished surfaces were ideally flat (on the length scale of the study). Then, by presuming insignificant chemical dissimilarity on the substrate surfaces prior to bonding, the values yielded a morphological toughening effect of 118 % (factor 2.2) and 90 % (factor 1.9) for the as-received and the etched surface condition (minimum 15 days storage), respectively.

Table 3.3. Experimental fracture toughness values based on the NCA fracture testing (Publication II); series average and ±standard deviation shown.

Substrate treatment	G_c for all specimens	G_c for minimum 15 days stored specimens
As-received	937 ± 537 J/m^2	643 ± 233 J/m^2
Etched	621 ± 211 J/m^2	560 ± 126 J/m^2
Electropolished	564 ± 523 J/m^2	295 ± 85 J/m^2

In Publication II, it was noted that the surface morphology of the substrates not only affected the average G_c values but also the nature of the

variation (in the values per series). For the specimens with the etched substrates, the stabilizing effect was not as clear as for the specimens with as-received and electropolished substrates, as shown in Fig. 3.6. The scatter in the values was attributed to the sharp surface shapes created by the nitric acid etching pre-treatment. It was concluded that the sharp ridges induced stress concentrations and resulted in premature crack initiation. Indeed, secondary cracks were occasionally found on the epoxy fracture surfaces of the etched specimens (Publication III). At any rate, to quantitatively define the nature of the scatter per test series, significantly larger test series would have been needed.

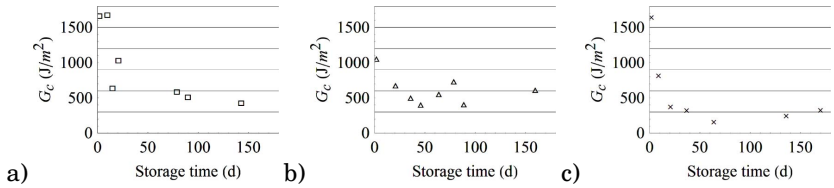

Figure 3.6. Critical energy release rate values as a function of specimen storage time: (a) specimens with as-received substrates; (b) specimens with etched substrates; (c) specimens with electropolished substrates.

Interface aging effect

The NCA testing revealed a significant decrease in the average G_c values (45–80%) when the bonded specimens were stored prior to testing. In Publication II, the degradation, or aging, was observed to have a stabilizing nature; the reduction in the values ceased after approximately 15 days of storage (see Fig. 3.6). Here, the storage refers to the time between the curing of the epoxy adhesive and the testing activity. Storage was arranged under prevailing laboratory conditions; the prevailing temperature and relative humidity (RH) were automatically recorded and the resulting mean values and standard deviation were 23 ± 2 °C, 32 ± 15 % RH (170 days).

The FM 300 epoxy adhesive, used in the bi-material specimens, is a commercial product developed to withstand high temperatures (up to 200 °C) and humid conditions. Studies on the mechanical properties and curing of this epoxy adhesive have been reported in the existing literature (e.g. Kohli, 1999; Djokic et al., 2001). Based on the literature, the adhesive's degree of cure has an upper limit for each isotherm cure temperature. Also, the T_g increases almost linearly when an upper limit for the degree

of cure is approached. For an isotherm cure temperature of 175 °C, the progress of the degree of cure ceases after approximately 50 minutes of cure. For the cure cycle that was applied here (Publications I–III), a peak temperature of 175 °C and a dwell time of 60 minutes were achieved. Hence, it is unlikely that either the degree of cure or T_g in the bulk epoxy could deviate after the specimen preparation and affect the NCA fracture test results reported in this thesis.

In Publication III, it was suggested that a thin interphase existed between the stainless steel's oxide coverage and the epoxy layer. This conclusion was made based on EDS and XPS compositional analysis as well as observations regarding the damage on fracture surfaces using AFM. For this, the interphase was conceptually defined as a function of the nitrogen content. For the aged specimens, the epoxy side of the fracture surface did not show any signs of nitrogen when using EDS. XPS in turn indicated higher nitrogen content on the epoxy fracture surface of an aged specimen (relative to the carbon content). Based on the approximate sampling depths of the two methods of analysis, a nitrogen-rich interphase was postulated with a thickness ranging from 10–20 nm to a maximum of 1 µm. In addition, AFM measurements revealed local micro-scale cracks and respective tearing of an interfacial layer with a thickness of 50–100 nm (see Fig. 3.7(a)); these findings supported the estimated thickness range of the interphase. The formation of the interphase was found to be the most likely factor responsible for the time-wise degradation of the fracture toughness values of the stainless steel-epoxy interfaces. When compared to the existing literature and the reported interphases on aluminium and titanium substrates (Bouchet et al., 1999; Possart et al., 2006), the suggested steel-epoxy interphase was very thin.

3.2.6 Description of the fracture process

In Publication III, the nature of the fracture process was studied using AE, FESEM and AFM. The AE measurements straightforwardly showed that the acoustic emission could not be observed during the interface fracture suggesting that the failure process zone was small. The combination of FESEM and AFM data showed that the fracture occurred along the interface at a micrometre level of accuracy. For fresh specimens (no storage), and especially for the as-received substrates, occasional local cohesive failure occurred at the grain boundary grooves (see Fig. 3.7(b)). No signs of friction or sliding by the delaminated epoxy layer were observed.

On a sub-micron scale, the fracture surfaces evidenced brittle fracture occurring presumably in the immediate vicinity of the stainless steel oxide coverage.

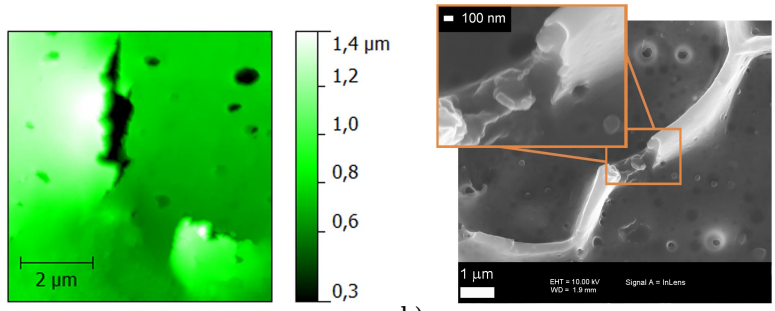

Figure 3.7. Local microscale damage on epoxy fracture surfaces: (a) shredding of a thin, interfacial layer; (b) cohesive failure at a narrow grain boundary groove.

3.3 Simulation of fracture along an interface with micro-roughness: Work conducted in Publication IV

The results presented in Publications I–III demonstrated that the interface strength of the stainless steel-epoxy bi-materials was affected by residual stresses, surface morphology and aging at the interface. However, it was not possible to quantitatively assess the share of each factor. In Publication IV, a numerical simulation was used to distinguish between the effects of each factor on the interface fracture. The aim was to simulate the interface fracture along a specific micro-roughness and under remote mode II dominant crack-tip loading as well as to directly analyse the resulting effects on the macroscopic behaviour of each factor—comparable studies do not exist in the current literature.

3.3.1 Interface model

The interface configuration with the as-received substrate condition (see Table 3.1) resulted in the highest apparent energy release rate and, henceforth, was chosen as the simulation basis. The grain boundary grooves on the as-received substrates represented types of roughness shapes that could increase adhesion based on the idea of crack meandering; depending on the wetting of the grooves by the epoxy adhesive and the chemical bonding to the groove edges, both peeling and shearing-type crack propagation would require additional amounts of energy.

The present fracture mechanics simulations in the existing literature, especially from the crack propagation point of view, can be divided into studies of two and three-dimensional cracks. Since the work at hand does not specifically concentrate on fracture mechanics, the two-dimensional view was chosen—since it is a simulation tool that is extensively supported in the existing literature. To create a numerical, two-dimensional model of the surface geometry, the morphology of the grooves was determined using AFM. Extracted AFM height data at different locations on a substrate were adopted for a generalized cross-sectional shape of a grain boundary groove, as illustrated in Fig. 3.8. The thickness of the stainless steel's oxide layer was far beyond the chosen length scale, i.e. the oxide layer was assumed not to have an effect on the stiffness of the real interface on a micro-scale. This also means that the interface was modelled in the form of an elementally discrete (compositional) boundary.

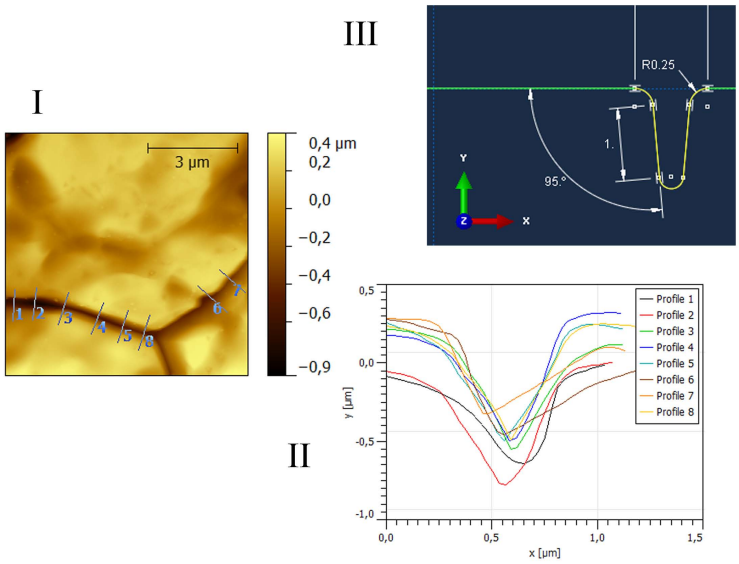

Figure 3.8. Schematic illustration of the process of determining generalized cross-sectional shape of a grain boundary groove. The third step shows the geometry being implemented for an FE model.

So-called sub-models, sometimes used to allocate calculation capacity for small-scale features, were not used in Publication IV due to problems with the boundary conditions when simulating crack growth (Towashiraporn et al., 2005). Instead, a specific *roughness block* was developed to compose a usable finite element simulation on a micro-scale. The roughness block is a separate geometry (body), which involves the interface with a single grain boundary groove. The interface was assigned to the VCCT

in order to simulate the crack propagation. The challenge in developing the roughness block was to create a mesh gradient that was smooth but also as steep as possible; the size ratio between the elements at the interface and at the free surfaces was more than one thousand. Also, reasonable convergence during the VCCT required careful mesh design along the interface. The simulation as a whole was divided into two steps: a residual stress step and a crack propagation step. Linear elasticity was assumed as a starting point; the justification for the linearity will be discussed in Section 3.3.3.

First, the usability of a single roughness block alone was studied. These results already have been reported previously (Kanerva et al., 2012). The use of a roughness block alone limits the extent of simulated crack propagation, and also the success of solving the calculation is sensitive to the applied load introduction and boundary conditions. Moreover, it is difficult to compare the simulation results with the experimental values determined on a macro-scale. Due to these deficiencies, an entire *specimen model* was developed. The specimen model consisted of two identical roughness blocks and two tab ends that formed the rest of the true-sized specimen, as shown in Fig. 3.9. The specimen outside both roughness blocks was simulated using a clearly coarser mesh but, even still, a realistic load introduction subjected to the tabs.

Residual stress model

Residual stresses were simulated by assuming linear thermal expansion and a uniform thermal load. The aim was to simulate the stress state and not the actual formation process of the residual stresses. However, it should be noted that the coefficient of thermal expansion (CTE) for the epoxy was determined experimentally during the work reported in Publication I and it was based on the same specimen geometry that was adopted for the full-scale specimen FE model. Therefore, the simulated residual stresses included the contribution of sources other than pure CTE mismatch, e.g., stresses due to cure shrinkage. An unfortunate consequence of the two-dimensional context is that the consideration of the third dimension is limited to two ideal categories, namely the plane-stress and plane-strain state. The limitations due to either the plane-stress or plane-strain state must be considered for the model in question, and the most important considerations for this thesis have been discussed previously by Kanerva et al. (2012). In addition, the effects of the two-

dimensional formulation of the NCA analysis have been reported by Dillard et al. (1999). The simulations reported in Publication IV assumed the plane-stress state, mostly because it resulted in a (more) realistic simulation of residual stresses; the plane-strain state caused an overly stiff lateral constraint and, consequently, unrealistic lateral residual stresses.

The initial residual stress simulations using a roughness block alone included considerations of a thin interphase. The interphase was modelled in the form of a discrete, 1-µm-thick section at the interface, on the polymer side. This section made is possible to adjust the Young's modulus and CTE of the interphase. However, realistic (but imaginary) deviations in the Young's modulus or CTE of the thin interphase did not result in significant differences in the behaviour of the interface (Kanerva et al., 2012). Thereafter, no interphase was simulated in the specimen model and considered for further studies. For the full-scale specimen model, the results of the residual stress simulation were compared with the analytical distribution (see Section 3.2.3) and found to be well matching. The simulated deformation shape of the bi-material specimen was a circular arc having a radius of 198 cm, which compared well to the experimental curvature measurements (209 cm, reported in Publication I).

Flaw model

A real interface, on a micro-scale, involves different types of flaws. In Publication IV, a local de-bond, or void, at the tip of a grain boundary groove was studied in the form of a micro-scale de-adhesion process. A void at the tip of the grain boundary groove was found to be realistic based on the fact that a grain boundary groove, in reality, can be sharp and might not be perfectly wetted by a high-viscosity epoxy during the bonding process. The voids at the groove tips were modelled by leaving the interface free at specific nodal points. The applied crack propagation technique, VCCT, also enabled crack propagation at the new crack tips, which formed due to the opening of the nodal contact. Therefore, it was possible to simulate an imperfect interface and secondary crack propagation.

3.3.2 Gradual fracture along micro-roughness

According to the simulations, the crack propagation along the interface, which occurred exactly at a grain boundary groove, was characterized by an M-shaped mode-mixity distribution, as shown in Fig. 3.10. An intense mode II peak appeared at the groove shoulders, whereas a strong mode I

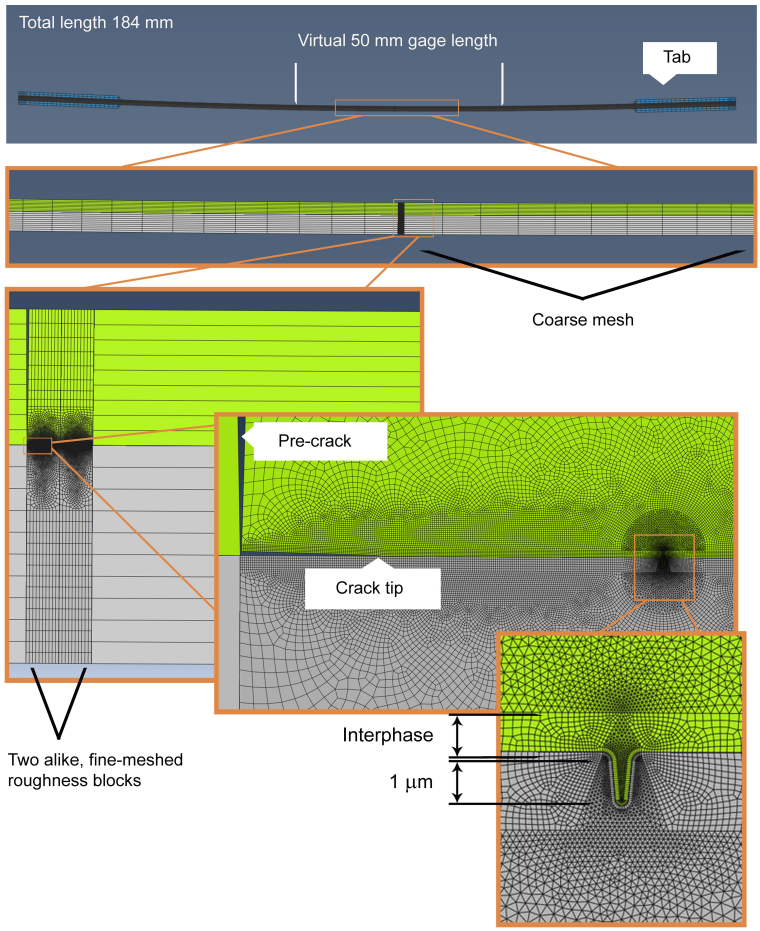

Figure 3.9. The full-scale specimen model developed for simulating interface fracture. The model consists of two fine-meshed roughness blocks and two coarse-meshed, tab-ended specimen arms.

contribution predominated during the crack growth towards the groove tip. This overall behaviour was found to be insensitive to the selection of the fracture criterion. Residual stresses directly affected the load (i.e. substrate strain), which was required in order to drive the crack along the interface. This residual stress effect is macroscopic and has been reported in the existing literature for several different fracture test specimens (Nairn, 2000; Guo et al., 2006).

Realistic deviations in the mode-specific critical energy release rates or power-law exponents did not significantly affect the mode-mixity distribution, i.e., the general behaviour of the fracture at the roughness shapes. Omitting the residual stresses (i.e. applying a zero thermal load) only led to a slight shift in the average mode-mixity (a 9% increase in the mode II dominance).

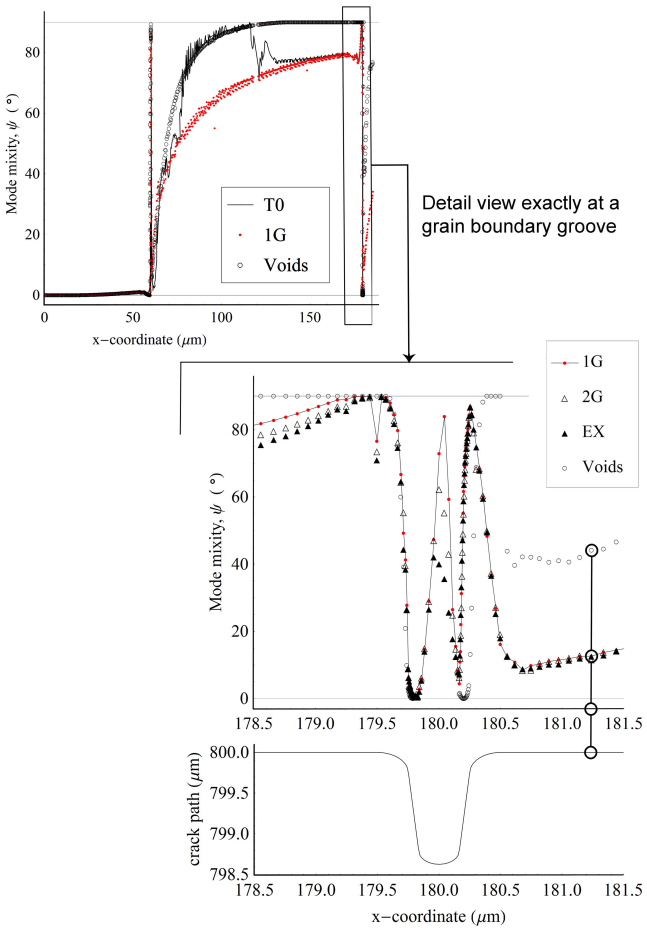

Figure 3.10. Crack-tip loading mode-mixity based on the simulations of crack propagation. The x-coordinate runs along the interface. In the graphs, T0 refers to zero thermal load, 1G refers to a fracture criterion assuming $G_{Ic} = G_{IIc}$, 2G refers to a general fracture criterion ($G_{Ic} \neq G_{IIc}$) and EX refers to a parabolic fracture criterion. The Voids curve refers to a fracture simulation along an imperfect interface.

The implementation of flaws at the groove tips had a significant effect on the interface fracture. In particular, an imperfect interface resulted in the initiation of secondary cracks. The propagation of a secondary crack finally led to crack coalescence at the time when the secondary crack reached the main crack front. This type of an interface collapse is totally different than the monotonic propagation of a single crack-tip. Because of the restricted crack opening during the propagation of the secondary crack, the average mode-mixity shifted by 20% towards the mode II dominance (average mode-mixity $\psi \approx 70.6\,^{\circ}$).

3.3.3 Engineering toughening factor

The experimentally measured strains (in Publication II) made it possible to assess the simulated energy release rate of the FE specimen model. Using the simulation, an energy release rate of 6.4 J/m^2 was estimated for the interface between the topmost stainless steel surface (assumed oxides) and epoxy on a *micro-scale*. A comparison of this value with the apparent critical energy release rate via NCA testing (643 J/m^2) indicated a significant, 100-fold toughening due to the grain boundary grooves. The ratio of experimental, apparent critical energy release rate and the iterated interface energy release rate on a micro-scale was defined as the *engineering toughening factor*. The crack coalescence due to voids decreased the critical load (substrate strain) by 16% and the toughening by 35%. In the event that voids initially extended to the groove walls (in addition to the groove tips), the toughening effect was completely lost; the groove shoulders alone did not introduce toughening.

In Publication IV, the linear elasticity of the epoxy and linear crack-tip displacements (inherent in VCCT) were justified based on the findings in Publication III. The fracture surfaces revealed brittle fracture and, thereby, suggested that the de-adhesion process occurred in a brittle manner either inside the stainless steel's oxide layer or along the interface between the oxide layer and the epoxy. Several studies in the existing literature have shown that, for the most part, the yielding of the (stiffer) substrate does not generally affect the macro-scale crack path at a bi-material interface in general and also that it does not affect the energy release rate during NCA testing (Tilbrook et al., 2005; Dillard et al., 1999). However, the yielding that occurs exactly at the grain boundaries is most probably an anisotropic phenomenon (Qi and Krajewski, 2007; Lenci and Wolski, 2012), and a simulation of this behaviour would require further studies using a partially discrete model.

3.4 Strength of composite-composite interfaces: Work conducted in Publications V–VI

The interfaces in composite systems were studied in Publications V and VI. Due to the lack of a clear understanding of the effects of peel ply surface treatments on composite surfaces and interfaces, studies of peel ply surface treatments in the existing literature were reviewed in Publica-

tion V. Publication VI focused on experiments with a glass-fibre-reinforced unsaturated polyester composite material and the interfaces that formed when a peel ply or a tear ply was used as a surface treatment method.

3.4.1 The peel ply surface treatment of composites: A literature review

In general, the surface treatments for polymeric substrates include mechanical abrading, blasting treatments, laser treatments, plasma treatments and chemical treatments. The free surfaces of fully conversed thermosetting polymers are relatively inert and their oxidation does not have a straightforward, advantageous effect on the bonding characteristics (Cognard, 2006). Fundamentally, polymer surfaces are inherently different than the bulk because of the lower conformational entropy forced by mould or free (air) surfaces; the molecular structure at the free surfaces prefers a lower molecular weight compared to the bulk (Sperling, 2006). The resulting deviations in the polymer's molecular weight presumably occur at the extreme surface. However, unwanted stoichiometric deviations at the surfaces can form wider (inter-) phases; species with a low molecular weight, e.g. excess co-reactant species, can easily migrate onto the free surfaces during long-term curing reactions. For example, hydrocarbon waxes are added to commercial unsaturated polyester resins to enhance the handling of composite products during manufacture (e.g. Ackermann, 1966) and these waxes have a tendency to migrate onto the surfaces during curing (Skrifvars et al., 1999; Davies et al., 2005). Therefore, surface treatments for cross-linked polymers aim to remove the low-molecular weight surface layer, including any possible impurities or an additive-rich coverage. The most straightforward means for doing this are mechanical abrading or, alternatively, applying of peel plies.

A peel ply is a fabric woven of polymeric fibres, and it is removed from the composite surface prior to bonding procedures. Removing of the peel ply strips away the outer surface and creates surface roughness. The peel ply's fibres are typically made of polyamide or polyester, although glass (Flinn et al., 2007) and aramid (Crane and Hamermesh, 1976) have also been used. In addition to these *dry* peel plies, a peel ply fabric can be pre-impregnated with a suitable thermosetting resin to form a special product (Molitor et al., 2001; Klapprott and Fox, 2010). The impregnated peel plies are termed *tear plies* (or wet plies) in the existing literature and commercial markets. Usually, the tear ply's impregnation resin is an epoxy

system with added plasticizers or toughening rubbery phases (Shah et al., 2010).

Surface condition of peel ply-treated surfaces

The morphology created by the peel ply is a systematic roughness pattern. The pattern is determined by the weaving, bundle size and fibre geometry (diameter) of the peel ply fabric. Bénard et al. (2005) reported that the level of (average) roughness on their peel ply-treated surfaces did not correlate with the resulting interface strength—especially in the case of practical, high-strength adhesive joints. In the case of (impractical) low-strength joints, the level of roughness tended to correlate with increased strength. Prolongo et al. (2010) studied composite surfaces that had been treated using different methods and they determined several roughness parameters based on the profilometry and scanning electron microscopy imaging. They were not able to find a significant, reliable correlation for any type of roughness parameter on the joint strength. The difficulty in relating surface roughness to joint strength has also been reported by Pocius and Wenz (1985).

Based on the existing literature, observations using X-ray photoelectron spectroscopy (XPS) and secondary-ion mass spectroscopy (SIMS) have been able to show that a polyamide peel ply treatment results in a surface with a relatively high amount of nitrogenous groups and relevant chemical bonds (Bénard et al., 2005; Phariss et al., 2005). Meanwhile, polyester peel plies result in surfaces with a richer occurrence of aromatic and oxygen aliphatic groups (Bénard et al., 2005). It has been found that a peel ply treatment increases the surface energy and affects the polarity of the treated composite surface (Bénard et al., 2007). Studies by Clark and Flinn (2007) and Bénard et al. (2005) strongly suggest that treatments using polyamide peel plies increase the polarity of a composite surface, while polyester peel plies result in somewhat less polar surfaces.

The above-mentioned compositional analysis and contact angle findings on treated composite surfaces imply that the observed increase in the polarity and population of nitrogenous species could be followed by enhanced wetting when using an adhesive during bonding. It should be noted that the effect of roughness and possible revealed fibres are superimposed on the results. Surface roughness is generally found to affect the surface energy values from contact angle data, and the effect is rather difficult to exclude (Bénard et al., 2007; Chin and Wightman, 1996).

Degree of cure of substrate composites

From the point of view of increased interdiffusion at an interface, a lower degree of cure is expected to have, without dispute, a favourable effect on the resulting interface strength in a bonded, fully cured joint. At best, the interpenetration between a substrate polymer and the adhering polymer can form a strong interphase or even heal the interface between two (similar) polymers. However, regardless of the intriguing idea of possible cross-linking through an interface, the effect of the substrate's degree of cure has not been soundly studied. Only a brief study by Flinn and Hickmott (2009) can be found; they studied the effect of the degree of cure on the interface fracture toughness of adhesively bonded, carbon fibre-epoxy composites. They prepared adherent laminates and controlled the degree of cure by adjusting the cure temperature and, ultimately, they bonded the laminates using a film adhesive. The degree of cure of the adherents was determined using DSC (prior to the cure of the adhesive film). They observed a 270% increase in fracture toughness for an 18% decrease in the adherent degree of cure. In practice, it is rather difficult to control exactly the degree of cure because, at a high level of degree of cure, the reactions of the condensation-type polymerization are sensitive to several different parameters, including temperature, pressure, co-reactants and the outgassing of small condensation species, such as water molecules (Odian, 2004). Also, slight deviations in the cure sequence of a curing polymer can affect the mechanical properties in the bulk and the residual stresses in a bonded system (Djokic et al., 2001). The difficulty from an industrial perspective has to do with the monitoring a controlled level of cure—not to mention preserving a level value in the event of storage.

The degree of cure is an important parameter for the peel ply treatments. Davies et al. (2005) studied the effect of preparation delays on overlaminated (i.e. bonding by matrix polymer) composite-composite joints. They observed a higher fracture toughness in joints with a delay period between the substrate preparation and joint overlamination phases. A study by Perrot et al. (2008) supports the time-dependency of success in preparing composite-composite joints using a peel ply surface treatment. In their study, a comparison was made between two different unsaturated polyester matrices, and it was concluded that the resin with a low styrene content was clearly more sensitive to the surface treatment procedures, including preparation delays.

Interphase formation

For molecular mobility, cross-linking reactions prior to bonding hinder the movement of species and, therefore, are disadvantageous when preparing strong, gradient interfaces. The impregnation resin of a tear ply is already in a partly cured state, i.e. in the so-called 'b-stage', which eases the handling of the tear ply when manufacturing composite parts. The interface formation that takes place during the tear ply pre-treatment can be divided into two stages. During the elevated temperature curing of a composite substrate, the impregnation resin merges with the composite's matrix resin and also a part of it will remain on the surface after removing the tear ply, as illustrated in Fig. 3.11(a). In theory, the ratio of the two polymer species shows a distribution in the direction perpendicular to the treated surface. Consequently, depending on the amount of interaction between the two species, possible interdiffusion will produce a gradient in the direction perpendicular to the bond surface.

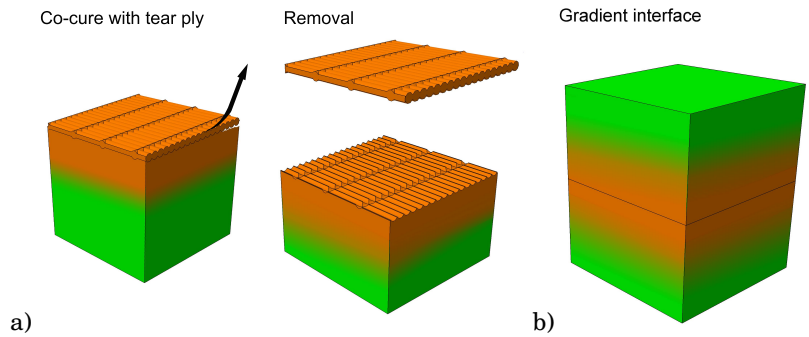

Figure 3.11. Tear ply surface treatment on a composite substrate: (a) curing of the composite lay-up and removal of the tear ply; (b) formation of a double-gradient interface during the bonding process, assuming interdiffusion.

After co-curing the substrate with the tear ply product, the resin-rich surface protects the composite's fibres from being revealed and affected by moisture and also isolates the surface from surrounding impurities. The toughness of the impregnation resin will also influence the formation of a strong interface after the tear ply removal and during the subsequent bonding preparations. If the treated surface is not fully cured at the time of bonding, gradients of molecular structure and mechanical properties might form on the side of the adhering polymer, as illustrated in Fig. 3.11(b). Unfortunately, there is not a single experimental study on the gradient interfaces of the composite joints pre-treated using a tear ply treatment available in the existing literature.

3.4.2 Modification of composite-composite interfaces for the thesis experiments

In general, an unsaturated polyester (UP) resin cure readily at room temperature, whereas the impregnation resin in a tear ply usually requires an elevated temperature cure (up to 190 °C). In Publication VI, the application of an epoxy resin-impregnated tear ply was experimentally studied as a surface pre-treatment for unsaturated polyester-glass composites. The idea in the use of the epoxy-impregnated tear ply as a pre-treatment for the unsaturated polyester-glass composites was to study the interphase formation between the impregnation resin and the unsaturated polyester. Typical peel plies were studied for the purpose of making comparisons and a stainless steel mesh was studied in order to estimate the effect of the raw material of the peel plies.

Peel ply-generated morphology

The different peel ply products studied in Publication VI are listed in Table 3.4. Based on FESEM imaging, the size (diameter) of the peel ply fibres and the amount of fractured matrix polymer on the treated composite surfaces were found to be essentially comparable (between the different products). The steel mesh had thicker 'fibres' and more open weaving. The absence of silicon and fluorine-based coatings was verified using EDS. Essentially, revealed glass-fibres (of the composite) were not observed on the treated surfaces.

The degree of cure on treated surfaces

Three different cure methods were studied when using the tear ply product, as described in Table 3.5. All three cure methods included an initial cure at room temperature and also a subsequent period, which was either continued at room temperature or carried out at an elevated temperature. The heating, when applied, was performed using an infrared heater (120 °C) or oven (140 °C). The length of the initial curing was seven hours and the subsequent period five hours. All of the test laminates were cured at the same time. After a total of 12 hours of curing, the tear ply (or peel ply) layers were stripped off and the second composite adherent was overlaminated on top of it using unsaturated polyester and the glass-fibre reinforcement (mat fabric). Before the overlamination, small laminate samples were cut for DSC measurements and stored in a refrigerator (–20 °C) to prevent further cure. The DSC samples were transported to

Table 3.4. List of the peel ply and tear ply products used for the composite surface treatment procedures (Publication VI)

Peel ply / tear ply	Fibre raw material	Fibre surface treatment	Impregnation resin	Cure
Release ply F by Airtech	Polyester	Heat-set and scoured, no release agent	-	-
A100PS by Richmond Aerovac	Polyamide	Heat-set and scoured, no release agent	-	-
M21/48%/F08111 by Hexcel	Polyester	Heat-set and scoured, no release agent	M21 toughened epoxy	up to 190 °C
Woven steel mesh by A.C.R.S. Co.	AISI 304	-	-	-

the instrument within three hours; meanwhile, they were kept at –10.3 through –19.5 °C using heat sinks and an insulated case. The degree of cure on the treated composite surfaces was determined to be 90.3%, 99.4% and 97.7%, respectively, for the room temperature cure, oven cure and infrared cure. Additionally, bare tear ply samples were cured using the two elevated-temperature methods (Table 3.5). For the tear ply samples, a degree of cure of 96.1% and 78.6% was determined for the oven cure and infrared cure, respectively. All of the (DSC) degree of cure values were calculated in relation to the exothermic heat of a tear ply sample in the b-stage, i.e. representing the tear ply's degree of cure after taking it out of the refrigerator.

The DSC analysis in Publication VI showed that the residual exothermic heat was directly dependent on the cure method being used. The values of the laminate surface samples were monotonically higher and indicated that catalytic reactions due to the composite's UP resin might have taken place (Lin et al., 1995, 1999). In addition to the high values of the degree of cure, the exothermic valley in the DSC curves of the laminate samples showed a broader shape and occasionally two peaks—suggesting two different species. It should be noted that the DSC samples from the laminate

Table 3.5. Description of the cure methods used for composite-composite joints with different surface treatments.

Peel ply product or surface treatment	Laminate cure for the first 7 hours	Laminate cure for the last 5 hours
Mechanical abrading after a total of 12 hours of cure (grade P36)	Ambient cond.	Ambient cond.
Release ply F	Ambient cond.	Ambient cond.
A100PS	Ambient cond.	Ambient cond.
M21/48%/F08111	Ambient cond.	Ambient cond.
M21/48%/F08111	Ambient cond.	Air circulating oven (140 °C)
M21/48%/F08111	Ambient cond.	Infrared heater (120 °C)
Steel mesh	Ambient cond.	Ambient cond.

surfaces included the UP matrix, which, in part, made the apparent degree of cure higher and might show up as a broader exothermic valley (i.e. initiating at a relatively low temperature).

A comparison of the tear ply treated surfaces from a pure morphology perspective showed a distinctive difference between the tear ply applications, as shown in Fig. 3.12. The cure at room temperature led to cavities (i.e. peel ply fibre-moulded cavities), which were fully patterned by microscopic pores. The pores were absent in the substrates treated using either of the two elevated-temperature cure methods. The fact that the pores existed primarily for the room temperature application indicates that the pores might have been the result of non-coherent curing of the UP and impregnation resin. The fast progression of the UP cure might have blocked the diffusion of gaseous species into the bulk composite. In turn, reaction coherency during an elevated temperature cure could have led to the formation of cleaner cavities without pores.

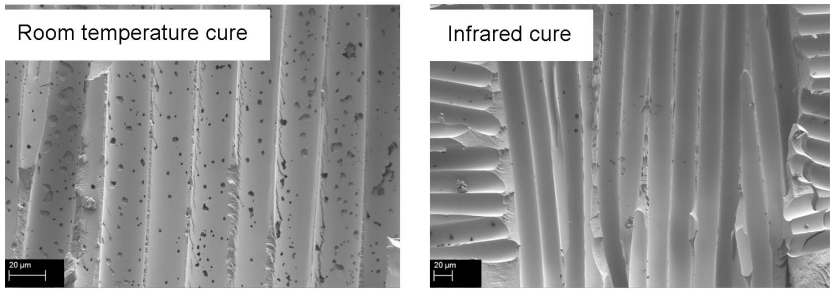

Figure 3.12. Composite surfaces pre-treated using a tear ply. The room temperature application (on the left) resulted in micro-pore formation, whereas elevated temperature applications, e.g. those using an infrared heater (on the right), led to cleaner cavities lacking any pores.

Characterization of the tear ply-modified interface

In Publication VI, the interface between the substrate composite and the overlamination composite was studied using cross-sectional microscopy. The samples were prepared by applying the ultramicrotomy sample preparation. For this, pieces were extracted from the bonded laminates using a small diamond saw (and cutting dry). These pieces were pre-shaped using a rotovator so that they would have a proper pyramidal shape prior to ultramicrotomy. The interface region in each piece was first shaped into a tapered shape, as is customary for this preparation technique. Lastly, the pyramidal region was smoothed using a virgin edge of a glass knife, a slow cutting speed (0.3–0.8 m/s) and thin slices (70–130 nm). During the preparation, no water or solvents were used. The challenge with ultramicrotomy is that the final quality of the surface (or slice) is dependent upon the toughness of the sample material. For the composite system studied in Publication VI, cooling of the cutting chamber during ultramicrotomy was not found to be useful; the brittleness of the UP was the major difficulty, although some soft, tough regions were observed near the interface—possibly due to a dissolved binder (polyvinyl acetate) from the glass fabric reinforcement.

The aim of characterizing the interface this way was to search for nitrogen-rich regions, which were expected due to the tear ply's epoxy-based impregnation resin. According to the tear ply's manufacturer, the bisphenol-F epoxy resin included polyamine co-reactants. No indication of nitrogen was found using general EDS scans (averaged over frames of 1500–90 000 μm^2), most likely due to the low sensitivity of EDS to nitrogen and the low nitrogen content when averaged over a large scanned

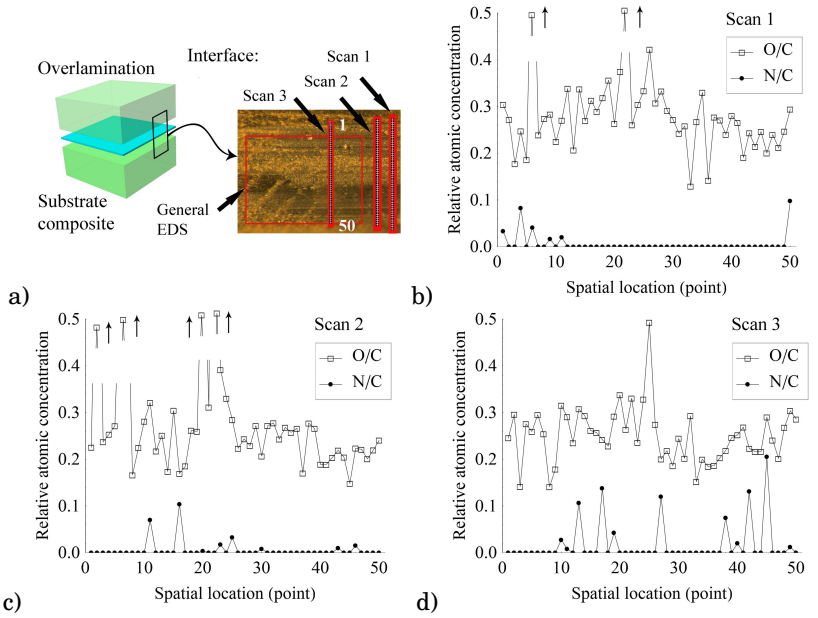

Figure 3.13. EDS line-scan spectra over the interface region of a tear ply pre-treated and room temperature-cured composite-composite joint: a) illustration of the sample and analysis locations; b) O/C and N/C distributions on scan no.1; c) O/C and N/C distributions on scan no.2; d) O/C and N/C distributions on scan no.3.

area. To find nitrogen locally, line-scan EDS was performed. A line-scan refers to a specific EDS technique where several points are analysed to determine a discrete (compositional) distribution along a single line. For each point analysis, the determined elemental content is representative of the material enclosed by a spherical volume under the electron beam and has a diameter of 1–2 µm. Because of this, there is a chance that a local trace of an element could be distinguished from the rest of the spectrum.

The line scans revealed nitrogen occurrence at the composite-composite interface, as shown in Fig. 3.13. The typical sizings applied to the carbon and glass fibres in composites are based on aminosilanes with epoxy and urethane components (Hughes, 1991; Mäder, 1997) and, therefore, could include nitrogen. The glass fibres used to reinforce the composites in Publication VI were analysed using EDS. The fibre surfaces were scanned at several locations and it was ascertained that no nitrogen was included on the fibre surfaces (so that it could affect the determined EDS spectra).

The EDS line scan spectra studied in Publication VI suggested that the co-reactant might have spread unevenly throughout the interface region. To assess the extent of spreading, the potential solid amount of impregnation resin, namely the solid thickness, was determined. Cross-sections

of a cured, bare tear ply piece were FESEM imaged; the sample pieces were cured on aluminium foil so that the impregnation resin formed a solid layer between the foil and the tear ply's fabric. The average solid thickness was determined to be 47.5 µm. In turn, the estimated average interphase thickness, based on the nitrogen traces of the line-scan data, was found to be 470 µm. By noting that the impregnation resin was in a gelled condition at the time of application, it was not found very probable that the impregnation resin could have diffused *evenly* into the UP resin over a volume ten times larger. However, the cross-sectional EDS analysis was not seen as a fully self-standing means for identifying the interphase and its thickness. Nevertheless, it should be noted that the moderate surface sensitivity of EDS is not a problem for a cross-sectional analysis so long as the interface structure is assumed to be continuous in the direction of the normal of the sample surface (i.e. two-dimensional).

3.4.3 Static strength and durability

In Publication VI, the interface strength of the different peel ply and tear ply pre pre-treated composite joints was screened using single-lap shear testing according to the ASTM D5868 standard. In order to provide an equal edge effect, round corners (with a 1.2 mm radius) were prepared to the edges of the overlap region using elastomeric moulds. All of the specimens went through a 48-hour post-cure sequence before testing—to ensure full cure of the UP resin at the time of testing.

The use of the tear ply treatment with either the intermediate oven cure or intermediate infrared cure resulted in a fully adhesive failure; FESEM imaging verified that the failure occurred exactly along the interface on a micro-scale (i.e. along the bond line). EDS analysis of a cross-sectional sample, which was cut from a tested specimen (overlamination side), indicated that no observable interphase had formed during the overlamination. The treatment using the dry polyester peel ply resulted in occasional adhesive failure, and was deemed an unreliable treatment. The mechanical abrading, stainless steel mesh, polyamide peel ply and epoxy-impregnated tear ply used with the room temperature application resulted in a fully cohesive failure inside the composite adherents (and for all of the specimens per series). Hence, the testing showed that the peel ply raw material as well as the degree of cure of the substrate composite prior to bonding had a clear effect on the interface strength. It was concluded that any intermediate curing (using an oven or infrared heater)

led to a higher degree of cure for the epoxy impregnation resin remaining on the composite surface and that the higher level of cure inhibited the overlamination resin from forming a strong interface.

In Publication VI, the four best performing interface configurations (defined under ambient conditions) were further studied using wedge testing. The wedge test specimens were conditioned using water immersion; distilled water and a nominal 64 °C temperature were applied for the conditioning. Prior inserting the stainless steel wedges, the test specimens were conditioned for two weeks. After inserting the wedges, the crack propagation was monitored while keeping the specimens immersed. In total, a 200-day conditioning period was considered. The results of the wedge testing, in terms of the energy release rate, G_I, are shown in Fig. 3.14. The energy release rate curves, calculated using Eq. 3.1, showed that only the treatments using either mechanical abrading or stainless steel mesh resulted in durable interfaces with slow crack propagation and a cohesive failure mode (crack-tip deflected into the composite material) during the water immersion at an elevated temperature. The performance of the stainless steel mesh treatment was also studied using DCB testing according to the ISO 15024 standard. In Publication VI, the results of the DCB testing (plus DCB specimens with *external load blocks* for wet specimens) showed that the stainless steel mesh pre-treated interface was strong after the entire conditioning period and also after drying the conditioned specimens; mode I energy release rate values (G_{Ip}) of 798 ± 164 J/m^2 and 885 ± 205 J/m^2 were determined for the wet and dried specimens, respectively. These values are clearly higher (but of the same order of magnitude) than the values reported in the existing literature (Davies et al., 2005; Perrot et al., 2008) for comparable adherent materials and surface pre-treatments.

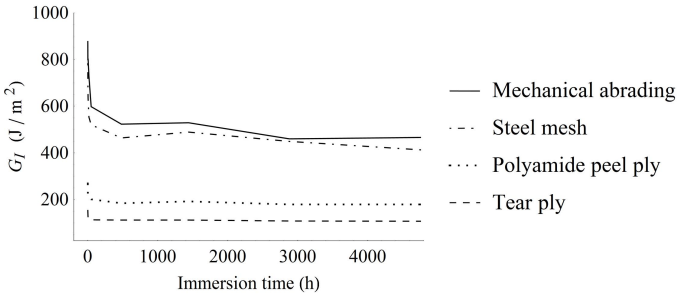

Figure 3.14. Results of the wedge testing of composite-composite interfaces with different pre-treatments; interface strength (energy release rate) as a function of water immersion time.

4. Summary and conclusions

4.1 Strength of rough stainless steel-epoxy interfaces

The strength of stainless steel-epoxy interfaces was experimentally studied in Publications I–II. In Publication I, substrate morphology was found to significantly affect the interface strength of the stainless steel-epoxy interfaces. In Publication II, the NCA fracture test method was applied to introduce mode II dominated crack-tip loading and the method made it possible to induce controlled interface fracture at a micrometre accuracy. Applying a systematic pre-crack preparation technique and studying strain rate profiles to determine the critical energy release rates revealed a three-phased interface fracture. A specific morphology affected the value of the critical strain energy release rate, its variation and also the initiation of secondary cracks on a sub-micron scale.

For many substrate materials, e.g. aluminium, the thickness of the oxide layer may reach 1 µm and the layer can chemically interact with the adhering polymer (epoxies) during the cure. The interaction between the surface oxides and the polymer's co-reactants presumably results in the formation of an interphase. Then, the formed interphase, with its own mechanical properties, represents the closest neighbour to the substrate on a micro-scale. In Publication III, it was hypothesized that the specific, slow formation of a thin interphase caused an aging effect. It was noted that the possible influence of the oxide layer should not be underestimated. Assuming that the macroscopic, apparent critical energy release rate for the electropolished substrate, determined in Publication III, was representative of a flat interface (lacking any roughness), the simulation results in Publication IV indicate that a deviation in the oxide layer on a nano-scale could increase the interface strength by a factor of approxi-

mately 50 (295 J/m^2 per 6.4 J/m^2).

The work reported in Publication I showed that thermal residual stresses at metal-polymer interfaces, on a micro-scale, follow the distributions calculated for a macroscopic specimen. Simulation results presented in Publication IV in turn verified the importance of implementing residual stresses in order to simulate a metal-polymer interface. However, it was noted that realistic residual stresses will not essentially change the nature of interface fracturing in terms of the mode-mixity at a specific micro-roughness, namely grain boundary grooves. Also, Publication IV verified that specific surface shapes on a micro-scale created specific interface loads, i.e. they modified the mode-mixity distribution at a crack-tip. In particular, the constant mode-mixity estimated analytically for a theoretical, level interface turned into a distribution where $\psi = 0\,^\circ ... 90\,^\circ$. These changes were the result of a crack meandering-type toughening mechanism at the grain boundary grooves. It should be noted that the intense and local mode II dominance ($\psi \approx 90\,^\circ$) at the grain boundary groove shoulders could indicate regions where the modelling accuracy on the selected length scale failed to simulate crack opening, friction or fracture mechanics of the oxide scale.

The interface model presented in Publication IV made it possible to iterate a value for the interface strength on a micro-scale, which could be distinguished from the apparent, macroscopic interface strength. An engineering toughening factor was defined as the ratio of these two values:

$$\frac{G_a}{G^{\Xi}} = f(length\,scale)\,, \tag{4.1}$$

where G_a is the apparent critical energy release rate, G^{Ξ} is the critical energy release rate omitting toughening mechanisms (i.e. it is defined by assuming a flat, structure-less interface on the selected length scale). The right-hand side of Equation 4.1 presents the engineering toughening factor as a function, which depends on the length scale of the modelled details. The author did not want to designate the engineering toughening factor via a specific symbol, simply to emphasize that the toughening factor should not be assimilated as an absolute measure or a single parameter. Instead, separate de-adhesion processes are to be modelled 'as they are' so that they generate the toughening effect within a simulation—this is the only way to correctly model the small-scale behaviour of interfaces, such as the crack coalescence or toughening effect by specific morphology. It is important to note that neither of the two energy release rates in Equation 4.1 are 'exact' or 'intrinsic'. First, G_a includes errors due to the

analysis of the conducted test and also possible measurement errors that resulted during the testing. For example, Equation 3.3 for the NCA test assumes negligible bending and that neither the substrate nor the delaminating polymer will yield. Second, the value of G^{Ξ} depends on the ambition of modelled details on the selected length scale. In other words, from the simulation and design perspective, interface strength can be thought to depend on the length scale considered. In Publication IV, the critical energy release rate of the interface (G^{Ξ}) was found to be 6.4 µN/µm for the stainless steel-epoxy interfaces on a micro-scale and the engineering toughening factor due to morphology was estimated to amount:

$$\frac{G_a}{G^{\Xi}} \approx 100\,. \tag{4.2}$$

In Publication IV, no oxide layer was modelled for the simulation due to the fact that its thickness for austenitic stainless steels was beyond the selected length scale. This means that any contribution of the oxide layer was included in G^{Ξ}.

In Publication II, it was reported that interface strength is not a stable quantity; instead, it is subjected to time-wise degradation, namely aging. Aging can refer to the influence of absorbed moisture, physical aging or chemical changes inside an interphase. Aging effects are important for metal-polymer interfaces as well as for polymer-polymer interfaces. In Publication II, a 45–80 % decrease in the (apparent) critical energy release rate of the interface was observed. Due to the significance of aging, the right-hand side of Equation 4.1 must be modified so that is is the form of a function of storage time (aging):

$$\frac{G_a}{G^{\Xi}} = f(length\,scale,\, storage)\,. \tag{4.3}$$

Another factor responsible for a significant length scale dependance is the material flaws. Flaws of different sizes were simulated in the work reported in Publication IV and it was found that relatively small adhesion flaws had a significant effect on the value of G^{Ξ} and the nature of interface failure. To date, not many studies have been done on the different types of flaws at interfaces and, hence, the analysis of the flaws' effect is mostly based on imaginary flaws.

The procedure for studying the factors affecting the interface strength of the stainless steel-epoxy system in Publications I-IV is summarized in Table 4.1.

Table 4.1. The procedure for studying the factors affecting the strength of stainless steel-epoxy interfaces.

Factor	Case material system: stainless steel-epoxy bi-material
Surface morphology	Critical energy release rate was directly dependent on the surface morphology of the stainless steel substrates. The shape of the grain boundary grooves was determined using AFM and a geometry was adopted for simulations. Deep, round-edged grain boundary grooves led to a toughening effect and increase in the apparent critical energy release rate value as well as an iterated energy release rate value from a numerical simulation using VCCT.
Oxide layer	The thickness of the oxide layer on stainless steel, in terms of an individual body, was beyond the selected length scale. Similarity in composition, on a micro-scale, was analysed using EDS.
Residual stresses	Residual stresses at the interface were studied using XRD. Residual stresses were taken into account in the calculated energy release rate on a specimen by specimen basis. Thermal residual stresses were validated and included in the interface fracture simulation.
Aging	Short-term aging was observed to decrease the interface strength and was addressed to formation of an interphase.
Flaws	Voids at the tip of grain boundary grooves were modelled. Simulation of voids indicated that relatively small flaws can entirely change the nature of interface fracture.

4.2 Strength of rough composite-composite interfaces

In Publications V–VI, planar composite-composite interfaces and substrate modifications were studied. The literature review reported in Publication V made it clear that the effect of roughness on the strength of polymeric composite-composite interfaces is not similar to the roughness effects on metal-polymer interfaces. The morphology of a polymeric substrate affects the resulting interface strength via an increased area for diffusion during surface wetting and it can also create mechanical interlocking. However, these effects of morphology are minor, e.g. when compared to the mechanical interlocking effect for metal-polymer interfaces. This is due to the inability of the compliant substrate to introduce toughening, such as elastic shielding or crack path deflection, unless the

Table 4.2. The procedure for studying the factors affecting the strength of composite-composite interfaces.

Factor	Case material system: Glass fibre-polyester composite
Surface morphology	Similar weaving and fibre geometry in the applied peel plies studied using FESEM resulted in essentially the same roughness pattern. Effects due to differences in morphology were negligible on the interface strength (based on literature).
Degree of cure	The degree of cure was determined using DSC. The degree of cure of the adherent surface directly affected the interface strength. A low value of the degree of cure increased the interface strength and hence was assumed to increase molecular diffusion of resin into the substrate during overlamination.
Post-cure and aging	All test specimens were post-cured to ensure an equal degree of cure prior to mechanical testing.
Surface chemistry	Peel ply fabrics were verified clean (un-coated) using EDS. Interface structure, due to addition of epoxy from a tear ply treatment, was studied using EDS on microtomed samples.
Moisture and temperature	The combined effects of moisture and elevated temperature on the interface strength were studied using fracture testing.

chemical bond is impractically weak.

Modification of a composite substrate refers to advantageous chemo-mechanical changes on the substrate's surface, e.g. removal of migrated, low molecular weight species, the addition of a toughening species in form of another polymer system, oxidation and also an increase in the surface free energy or polarity via surface treatments. In Publication VI, the addition of a toughening epoxy phase by applying a tear ply surface treatment was studied. The influence of the substrate modification using a tear ply was found to depend on the cure method prior to an overlamination process. Intermediate cure methods led to a higher degree of cure on the substrate's surface and impeded the formation of a strong interface during the overlamination process. In contrast, a low degree of cure increased the extent of reactions as well as diffusion into the substrate and resulted in a strong interface (in terms of shear strength and when determined under ambient conditions). However, a durability study using fracture testing and water immersion, reported in Publication VI, showed

that moisture absorbtion at an elevated temperature led to a substantial reduction in the strength of the peel ply-modified composite-composite interfaces. In contrast, further research could focus on a specific composite surface treatment using a stainless steel mesh, which, in addition to the systematic surface morphology, led to promising results in terms of fracture toughness and durability. The procedure for studying the factors affecting the interface strength of the composite-composite system reported in Publication VI is summarized in Table 4.2.

4.3 Conclusions

In this thesis, rough interfaces, i.e. interfaces formed on rough substrates, were studied. The thesis consists of two parts: the first part analysed a stainless steel-epoxy interface and the second part analysed planar interfaces in fibre-reinforced composite materials. The work done in the thesis concentrated on determining the influence of roughness on the mechanical strength of interfaces. The new findings of the thesis are as follows:

- Determined residual stresses at stainless steel-epoxy interfaces at a micrometre level of accuracy.

- A new operator-independent definition for the critical strain of interface collapse during the NCA testing that is based on strain-rate profiles.

- Observations of the short-term aging effect on critical strain energy release rate values under ambient laboratory conditions for stainless steel-epoxy interfaces and considerations of the migration of co-reactant species at a sub-micron scale interphase.

- Numerical simulation of mode II dominant interface fracture and an estimation of the share of grain boundary groove-induced roughness in terms of the critical strain energy release rate and also the established engineering toughening factor in order to compare the toughening effect with the experimental, macroscopic energy release rate value.

- The effect of peel ply raw material on the durability of composite-composite interfaces based on the results of fracture testing and with respect to pre-treatments using AISI 304 mesh and polymeric peel plies.

In this thesis, an experimental-numerical procedure for analysing the effect of a precise morphology was developed, as described in Fig. 4.1. As a future study, the developed procedure could be used to optimize the geometry of microscopic grain boundary grooves in order to maximize the resulting toughening effect in a macroscopic specimen, as presented in Fig. 4.1. Additionally, since it was found that the peel ply surface treatment creates a systematic, reproducible roughness pattern, a peel ply-modified composite-composite interface could work as a convenient starting point for simulating a fully polymeric interface. However, the fracture experimentation as well as the characterization of composite-composite interfaces require a further, intensive effort.

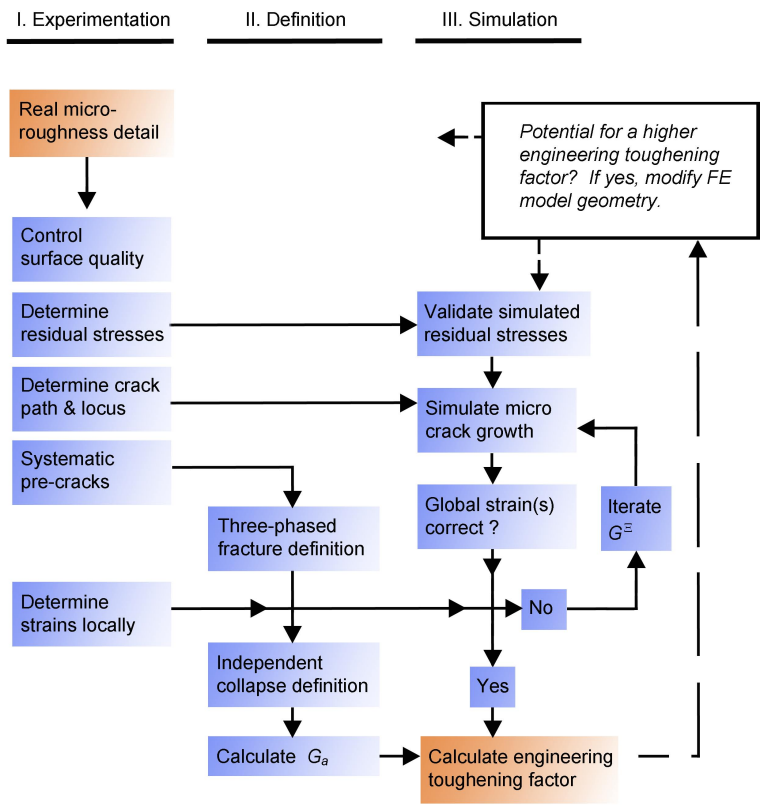

Figure 4.1. The experimental-numerical procedure developed in this thesis for analysing microscopically rough interfaces. The dashed lines show a potential scheme for a future study on the sensitivity of G^{Ξ} to modification of the roughness geometry for toughening optimization.

Bibliography

Abreu, C., Cristóbal, M., Losada, R., Nóvoa, X., Pena, G., and Pérez, M. (2004). Comparative study of passive films of different stainless steels developed on alkaline medium. *Electrochim Acta*, 49(17-18):3049–3056.

Ackermann, G. (1966). Thermosetting compatible petroleum wax-unsaturated polyester resin composition. United States Patent and Trademark office. United States patent no. 3249615.

Adamson, A. (1990). *Physical chemistry of surfaces*. Wiley, NY. 5th ed.

Andreikiv, O., Skal's'kyi, V., and Serhienko, O. (2001). Acoustic-emission criteria for rapid analysis of internal defects in composite materials. *Mater Sci*, 37(1):106–117.

Aufray, M. and Roche, A. (2006). Residual stresses and practical adhesion: Effect of organo-metallic complex formation and crystallization. *J Adhes Sci Technol*, 20(16):1889–1903.

Baldan, A. (2004). Adhesively-bonded joints and repairs in metallic alloys, polymers and composite materials: Adhesives, adhesion theories and surface pretreatment. *J Mater Sci*, 39(1):1–49.

Baldan, A. (2012). Adhesion phenomena in bonded joints. *Int J Adhes Adhes*, 38(1):95–116.

Balkova, R., Holcnerova, S., and Cech, V. (2002). Testing of adhesives for bonding of polymer composites. *Int J Adhes Adhes*, 22(4):291–295.

Basu, S., Mahajan, D., and Van Der Giessen, E. (2005). Micromechanics of the growth of a craze fibril in glassy polymers. *Polymer*, 46(18):7504–75018.

Beckit, F., Bastow, B., and Gladman, T. (1988). Effects of residual element contents on corrosion resistance of type 304L stainless steels in boiling nitric acid. In *Stainless steels '87 (Proceedings)*, pages 234–246. The Institute of Metals, London, UK.

Bélan, F., Bellenger, V., and Mortaigne, B. (1997). Hydrolytic stability of unsaturated polyester networks with controlled chain ends. *Polym Degrad Stab*, 56(1):93–102.

Bénard, Q., Fois, M., and Grisel, M. (2005). Peel ply surface treatment for composite assemblies: Chemistry and morphology effects. *Compos Part A Appl Sci Manuf*, 36(11):1562–1568.

Bénard, Q., Fois, M., and Grisel, M. (2007). Roughness and fibre reinforcement effect onto wettability of composite surfaces. *Appl Surf Sci*, 253(10):4753–4758.

Bentadjine, S., Petiaud, R., Roche, A., and Massardier, V. (2001). Organo-metallic complex characterization formed when liquid epoxy-diamine mixtures are applied onto metallic substrates. *Polymer*, 42(14):6271–6282.

Blomqvist, J. (2012). *Modeling of polymer-metal hybrid materials*. PhD thesis, Aalto University. ISBN 978-952-60-4775-1.

Bordes, M., Davies, P., Cognard, J.-Y., Sohier, L., Sauvant-Moynot, V., and Galy, J. (2009). Prediction of long term strength of adhesively bonded steel/epoxy joints in sea water. *Int J Adhes Adhes*, 29(6):595–608.

Bouchard, P., Bay, F., and Chastel, Y. (2003). Numerical modelling of crack propagation: Automatic remeshing and comparison of different criteria. *Comput Methods Appl Mech Eng*, 192(35-36):3887–3908.

Bouchet, J., Roche, A., and Hamelin, P. (1999). Internal stresses, young's modulus and practical adhesion of organic coatings applied onto 5754 aluminum alloy. *Thin Solid Films*, 355:270–276.

Bouquet, F., Cuntz, J., and Coddet, C. (1992). Influence of surface treatments on the durability of stainless steel sheets bonded with epoxy. *J Adhes Sci Technol*, 6(2):233–242.

Brown, S. and Pilla, G. (1982). Titanium surface treatments for adhesive bonding. Technical Report NADC-82032-60, Naval Air Systems Command, USA.

Bucknall, C. (2007). New criterion for craze initiation. *Polymer*, 48(4):1030–1041.

Chai, H. (2003). Interfacial mixed-mode fracture of adhesive bonds undergoing large deformation. *Int J Solids Struct*, 40(1):6023–6042.

Charkaluk, E., Bigerelle, M., and Iost, A. (1998). Fractals and fracture. *Eng Fract Mech*, 61(1):119–139.

Chen, B. and Dillard, D. (2001). Numerical analysis of directionally unstable crack propagation in adhesively bonded joints. *Int J Solids Struct*, 38(38-39):6907–6924.

Chen, B., Dillard, D., Dillard, J., and Clark Jr., R. (2001). Crack path selection in adhesively-bonded joints: The role of material properties. *J Adhes*, 75(4):405–434.

Cheuk, P. and Tong, L. (2002). Failure of adhesive bonded composite lap shear joints with embedded precrack. *Compos Sci Technol*, 62(7-8):1079–1095.

Chin, J. and Wightman, J. (1996). Surface characterization and adhesive bonding of toughened bismaleimide composites. *Compos Part A Appl Sci Manuf*, 27(6):419–428.

Clark, B. and Flinn, B. (2007). Evaluation of nylon and polyester peel plies using the rapid adhesion test. In *International SAMPE Symposium and Exhibition (Proceedings)*, Baltimore, USA. June 3-7.

Cognard, J. (2006). Some recent progress in adhesion technology and science. *C R Chim*, 9(1):13–24. (SPEC. ISS.).

Cooper, L. (2000). A role for surface topography in creating and maintaining bone at titanium endosseous implants. *J Prosthet Dent*, 84(5):522–534.

Cordisco, F., Zavattieri, P., Hector Jr., L., and Bower, A. (2012). Toughness of a patterned interface between two elastically dissimilar solids. *Eng Fract Mech*, 96(1):192–208.

Crane, L. and Hamermesh, C. (1976). Surface treatment of cured epoxy graphite composites to improve adhesive bonding. *Sampe Journal*, 12(2):6–9.

Davies, P., Baley, C., Loaec, H., and Grohens, Y. (2005). Interlaminar tests for marine applications. evaluation of the influence of peel plies and fabrication delays. *Appl Compos Mat*, 12(5):293–307.

De'Nève, B., Delamar, M., Nguyen, T., and Shanahan, M. (1998). Failure mode and ageing of steel/epoxy joints. *Appl Surf Sci*, 134(1-4):202–212.

Dillard, D., Chen, B., Chang, T., and Lai, Y.-H. (1999). Analysis of the notched coating adhesion test. *J Adhes*, 69(1-4):99–120.

Djokic, D., Johnston, A., Rogers, A., Lee-Sullivan, P., and Mrad, N. (2001). Residual stress development during the composite patch bonding process: Measurement and modeling. *Compos Part A Appl Sci Manuf*, 33(2):277–288.

Drefs, T., Webb, E., Ma, D., Alameda, J., Braatz, R., and Alkire, R. (2004). Coupled mesoscale-continuum simulations of copper electrodeposition in a trench. *Mat Interfaces Electrochem Phenom*, 50(1):226–240.

Elices, M., Guinea, G., Gómez, J., and Planas, J. (2002). The cohesive zone model: Advantages, limitations and challenges. *Eng Fract Mech*, 69(2):137–163.

Erdogan, F. (1965). Stress distribution in bonded dissimilar material with cracks. *J Appl Mech, Transactions ASME*, 32(2):403–410.

Erdogan, F. and Sih, G. (1963). On crack extension in plates under plane loading and transverse shear. *J Basic Eng, Transactions ASME*, 85(4):519–525.

Evans, A. (2006). *Adhesion Measurements of Films and Coatings*, volume 2, chapter Interface adhesion: Measurement and analysis, pages 1–18. VSP, Utrecht. Ed. K. Mittal.

Feraren, P. and Jensen, H. (2004). Cohesive zone modelling of interface fracture near flaws in adhesive joints. *Eng Fract Mech*, 71(15):2125–2142.

Fleck, N., Hutchinson, J., and Suo, Z. (1991). Crack path selection in a brittle adhesive layer. *Int J Solids Struct*, 27(13):1683–1703.

Flinn, B., Clark, B., Satterwhite, J., and Van Voast, P. (2007). Influence of peel ply type on adhesive bonding of composites. In *International SAMPE Symposium and Exhibition (Proceedings)*, Baltimore, USA. June 3-7.

Flinn, B. and Hickmott, C. (2009). Effect of surface preparation technique on bond quality of agate composite laminates. In *International SAMPE Symposium and Exhibition (Proceedings)*, Baltimore, USA. May 18-21.

Gent, A. and Lin, C. (1990). Model studies of the effect of surface roughness and mechanical interlocking on adhesion. Technical Report 25 (AD-A222 402), Office of Naval Research, USA.

Gent, A. and Schultz, J. (1972). Effect of wetting liquids on the strength of adhesion of viscoelastic material. *J Adhes*, 3(4):281–294.

Giese, J., Wu, W., and van Oss, C. (1996). Surface and electrokinetic properties of clays and other mineral particles, untreated and treated with organic or inorganic cations. *J Disper Sci Technol*, 17(5):527–547.

Giunta, R. and Kander, R. (2002). Accelerated aging of polyimide/titanium adhesive bonds using the notched coating adhesion test. *Polym Eng Sci*, 42(8):1789–1797.

Goldstein, R. and Salganik, R. (1974). Brittle fracture of solids with arbitrary cracks. *Int J Fract*, 10(1):507–523.

Gu, X., Raghavan, D., Nguyen, T., VanLandingham, M., and Yebassa, D. (2001). Characterization of polyester degradation using tapping mode atomic force microscopy: Exposure to alkaline solution at room temperature. *Polym Degrad Stab*, 74(1):139–149.

Guo, S., Dillard, D., and Nairn, J. (2006). Effect of residual stress on the energy release rate of wedge and dcb test specimens. *Int J Adhes Adhes*, 26(4):285–294.

Honkanen, M., Vippola, M., and Lepistö, T. (2011). Characterisation of stainless steel surfaces—modified in air at 350 °C. *Surf Eng*, 27(5):325–331.

Hughes, J. (1991). The carbon fibre/epoxy interface-a review. *Compos Sci Technol*, 41(1):13–45.

ISO (2001). Fibre-reinforced plastic composites—determination of mode I interlaminar fracture toughness, G_{Ic}, for unidirectionally reinforced materials. Standard no. 15024. International Organization for Standardization (ISO).

Janarthanan, V., Garrett, P., Stein, R., and Srinivasarao, M. (1997). Adhesion enhancement in immiscible polymer bilayer using oriented macroscopic roughness. *Polymer*, 38(1):105–111.

Jancar, J. (2008). Review of the role of the interphase in the control of composite performance on micro- and nano-length scales. *J Mater Sci*, 43(20):6747–6757.

Johansson, L.-S. (2002). Monitoring fibre surfaces with XPS in papermaking processes. *Mikrochim Acta*, 138-139(138/3-4,139/1-4):217–223.

Johnston, K. and Harmandaris, V. (2013). Hierarchical simulations of hybrid polymer solid materials. *Soft Matter*, 9(1):6696–6710.

Kanerva, M., Jokinen, J., and Saarela, O. (2012). Interface fracture study of substrate micro-roughness using atomic force microscopy and finite element analysis. In *Interface-21 international conference on composite interfaces (Proceedings)*, Kyoto, Japan. August 6-8.

Kim, W.-S., Yun, I.-H., Lee, J.-J., and Jung, H.-T. (2010). Evaluation of mechanical interlock effect on adhesion strength of polymermetal interfaces using micro-patterned surface topography. *Int J Adhes Adhes*, 30(6):408–417.

Kinloch, A., Little, M., and Watts, J. (2000). Role of the interphase in the environmental failure of adhesive joints. *Acta mater*, 48(18-19):4543–4553.

Klapprott, D. and Fox, L. (2010). Pre-impregnated peel ply systems—the range and breadth of usefulness as a surface preparation method for composite bonding. In *International SAMPE Symposium and Exhibition (Proceedings)*, Seattle, USA. May 17-20.

Kohli, D. (1999). Improved 121 °C curing epoxy film adhesive for composite bonding and repair applications: FM 300-2 adhesive system. *Int J Adhes Adhes*, 19(2):231–242.

Kolman, D., Ford, D., Butt, D., and Nelson, T. (1997). Corrosion of 304 stainless steel exposed to nitric acid-chloride environments. *Corros Sci*, 39(12):2067–2093.

Köver, L., Kádár, I., Cserny, I., and Tóth, J. (1983). XPS investigation of stainless steel surfaces heated in aqueous media. *Vacuum*, 33(1-2):99–105.

Krueger, R. (2004). Virtual crack closure technique: History, approach, and application. *Appl Mech Rev*, 57(2):109–143.

Legghe, E., Aragon, E., Bélec, L., Margaillan, A., and Melot, D. (2009). Correlation between water diffusion and adhesion loss: Study of an epoxy primer on steel. *Prog Org Coat*, 66(3):276–280.

Lenci, M. and Wolski, K. (2012). Quantitative analysis of grain boundary sliding by atomic force microscopy for early detection of intergranular damage. *Mater Sci Eng A*, 556:775–782.

Lin, C.-C., Hu, C.-C., and Lee, T.-C. (2009). Electropolishing of 304 stainless steel: Interactive effects of glycerol content, bath temperature, and current density on surface roughness and morphology. *Surf Coat Technol*, 204(4):448–454.

Lin, M.-S. and Chang, R.-J. (1992). Chemorheology on simultaneous ipn formation of epoxy resin and unsaturated polyester. *J Appl Polym Sci*, 46(5):815–827.

Lin, M.-S., Chang, R.-J., Yang, T., and Shih, Y.-F. (1995). Kinetic study on simultaneous interpenetrating polymer network formation of epoxy resin and unsaturated polyester. *J Appl Polym Sci*, 55(12):1607–1617.

Lin, M.-S., Liu, C.-C., and Lee, C.-T. (1999). Toughened interpenetrating polymer network materials based on unsaturated polyester and epoxy. *J Appl Polym Sci*, 72(4):585–592.

Loh, W., Crocombe, A., Abdel Wahab, M., and Ashcroft, I. (2002). Environmental degradation of the interfacial fracture energy in an adhesively bonded joint. *Eng Fract Mech*, 69(18):2113–2128.

Lothongkum, G., Chaikittisilp, S., and Lothongkum, A. (2003). XPS investigation of surface films on high cr-ni ferritic and austenitic stainless steels. *Appl Surf Sci*, 218(1-4):202–209.

Lothongkum, G., Klinkeson, A., and Jivavibul, P. (1999). XPS investigation of the 304L stainless steel surface film component after treating in hydrochloric,

sulfuric and nitric acid solutions at room temperature. In *International Corrosion Congress (Proceedings)*, Cape Town, South Africa. September-October 26-1.

Mäder, E. (1997). Study of fibre surface treatments for control of interphase properties in composites. *Compos Sci Technol*, 57(8):1077–1088.

Malik, M., Choudhary, V., and Varma, I. (2000). Current status of unsaturated polyester resins. *J Macromol Sci Polym Rev*, 40(2-3):139–165.

Mammoli, A., Graham, A., Reimanis, I., and Tullock, D. (1995). The effect of flaws on the propagation of cracks at bi-materials inferfaces. *Acta Metall Mater*, 43(3):1149–1156.

Maurice, V., Yang, W., and Marcus, P. (1996). XPS and STM study of passive films formed on Fe-22Cr(110) single-crystal surfaces. *J Electrochem Soc*, 143(4):1182–1200.

Móczó, J., Renner, K., and Pukánszky, B. (2012). Polarity, wetting, compatibility, interaction in polymer composites: facts and beliefs. In *Interface-21 international conference on composite interfaces (Proceedings)*, Kyoto, Japan. August 6-8.

Molitor, P., Barron, V., and Young, T. (2001). Surface treatment of titanium for adhesive bonding to polymer composites: A review. *Int J Adhes Adhes*, 21(2):129–136.

Mróz, K. and Mróz, Z. (2010). On crack path evolution rules. *Eng Fract Mech*, 77(11):1781–1807.

Mubashar, A., Ashcroft, I., Critchlow, G., and Crocombe, A. (2009). Moisture absorption-desorption effects in adhesive joints. *Int J Adhes Adhes*, 29(8):751–760.

Nairn, J. (2000). Energy release rate analysis for adhesive and laminate double cantilever beam specimens emphasizing the effect of residual stresses. *Int J Adhes Adhes*, 20(1):59–70.

Naito, K. and Fujii, T. (1995). Fractals for fractured surfaces of adhesives under static and fatigue loadings. *Int J Adhes Adhes*, 15(3):123–130.

Neumann, D. (1981). Styrene suppressed unsaturated polyester resin compositions. United States Patent and Trademark office. United States patent no. 4269745.

Nikolov, S., Han, C.-S., and Raabe, D. (2007). On the origin of size effects in small-strain elasticity of solid polymers. *Int J Solids Struct*, 44(5):1582–1592.

O'Day, M., Nath, P., and Curtin, W. (2006). Thin film delamination: A discrete dislocation analysis. *J Mech Phys Sol*, 54(10):2214–2234.

Odian, G. (2004). *Principles of polymerization*, chapter Step polymerization, pages 39–185. Wiley, Hoboken, USA.

Packham, D. (1986). Preparation of metallic surfaces with microfibrous topography and their effect on adhesion of hot-melt and thermoset adhesives. *Int J Adhes Adhes*, 6(4):225–228.

Packham, D. (2003). Surface energy, surface topography and adhesion. *Int J Adhes Adhes*, 23(6):437–448.

Palaniswamy, K. and Knauss, W. (1978). *Mechanics today*, volume 4, chapter On the problem of crack extension in brittle solids under general loading, pages 87–148. Pergamon. Ed. S. Nemat-Nasser.

Papanicolaou, G., Bouboulas, A., and Anifantis, N. (2009). Thermal expansivities in fibrous composites incorporating hybrid interphase regions. *Compos Struct*, 88(4):542–547.

Parnes, R. (2001). *Solid mechanics in engineering*. Wiley, Chichester, UK.

Partini, M. and Pantani, R. (2007). Ftir analysis of hydrolysis in aliphatic polyesters. *Polym Degrad Stab*, 92(8):1491–1497.

Perrot, Y., Davies, P., Kerboul, A., and Baley, C. (2008). Marine composites based on low styrene content resins. influence of lamination procedure and peel plies on interlaminar resistance. *Appl Compos Mat*, 15(2):87–97.

Persson, B. and Tosatti, E. (2001). The effect of surface roughness on the adhesion of elastic solids. *J Chem Phys*, 115(1):5597–5610.

Phariss, M., Flinn, B., Ballien, B., Grace, W., and Van Voast, P. (2005). Evaluation of peel-ply materials on composite bond quality. In *International SAMPE Technical Conference (Proceedings)*, Seattle, USA. October-November 31-3.

Pocius, A. and Wenz, R. (1985). Mechanical surface preparation of graphite-epoxy composite for adhesive bonding. *Sampe Journal*, 21(5):50–58.

Ponto, L., Datta, M., and Landolt, D. (1987). Electropolishing of iron-chromium alloys in phosphoric acid-sulphuric acid electrolytes. *Surf Coat Technol*, 30(3):265–276.

Possart, W., Krüger, J., Wehlack, C., Müller, U., Petersen, C., Bactavatchalou, R., and Meiser, A. (2006). Formation and structure of epoxy network interphases at the contact to native metal surfaces. *C R Chim*, 9(1):60–79.

Prikryl, R., Cech, V., Balkova, R., and Vanek, J. (2003). Functional interlayers in multiphase materials. *Surf Coat Technol*, 174-175:858–862.

Prolongo, S., Gude, M., Del Rosario, G., and Ureña, A. (2010). Surface pretreatments for composite joints: Study of surface profile by sem image analysis. *J Adhes Sci Technol*, 24(11-12):1855–1867.

Qi, G., Barhorst, A., Hashemi, J., and Kamala, G. (1997). Discrete wavelet decomposition of acoustic emission signals from carbon-fiber-reinforced composites. *Compos Sci Technol*, 57(4):389–403.

Qi, Y. and Krajewski, P. (2007). Molecular dynamics simulations of grain boundary sliding: The effect of stress and boundary misorientation. *Acta mater*, 55(5):1555–1563.

Reedy, E. (2008). Effects of patterned nanoscale interfacial roughness on interfacial toughness: A finite element analysis. *J Mat Res*, 23(11):3056–3065.

Reedy, E., Moody, N., Zimmerman, J., Zhou, X., Kennedy, M., Mook, W., and Bahr, D. (2007). Effect of nanoscale patterned interfacial roughness on interfacial toughness. Technical Report SAND 2007-5990, Sandia National Laboratories, USA.

Reid, A. and Gooding, R. (1992). Inclusion problem in a two-dimensional nonlocal elastic solid. *Phys Rev B*, 46(10):6045–6049.

Ritchie, R. (1988). Mechanisms of fatigue crack propagation in metals, ceramics and composites: role of crack tip shielding. *Mat Sci Eng*, A103:15–28.

Ritchie, R. (2011). The conflicts between strength and toughness. *Nature Mat*, 10:817–822.

Rouw, A. (1998). Model epoxy powder coatings and their adhesion to steel. *Prog Org Coat*, 34(1-4):181–192.

Roy, S., Darque-Ceretti, E., Felder, E., and Monchoix, H. (2007). Cross-sectional nanoindentation for copper adhesion characterization in blanket and patterned interconnect structures: Experiments and three-dimensional FEM modeling. *Int J Fract*, 144(1):21–33.

Ryoji, Y., Jin-Qiao, L., Jin-Quan, X., Toshiaki, O., and Tomoyoshi, O. (1994). Mixed mode fracture criteria for an interface crack. *Eng Fract Mech*, 47(3):367–377.

Sanderson, T. (2008). On the evaluation of residual stresses in bi-layer materials using the bent strip method. *Surf Coat Technol*, 202(8):1493–1501.

Sargent, J. (1994). Adherend surface morphology and its influence on the peel strength of adhesive joints bonded with modified phenolic and epoxy structural adhesives. *Int J Adhes Adhes*, 14(1):21–30.

Sause, M., Müller, T., Horoschenkoff, A., and Horn, S. (2012). Quantification of failure mechanisms in mode-I loading of fiber reinforced plastics utilizing acoustic emission analysis. *Compos Sci Technol*, 72(2):167–174.

Schuecker, C. and Davidson, B. (2000). Evaluation of the accuracy of the four-point bend end-notched flexure test for mode II delamination toughness determination. *Compos Sci Technol*, 60(11):2137–2146.

Sekulic, A. and Curnier, A. (2010). Experimentation on adhesion of epoxy. *Int J Adhes Adhes*, 30(2):89–104.

Sen, D., Thaulow, C., Schieffer, S., Cohen, A., and Buehler, M. (2010). Atomistic study of crack tip cleavage to dislocation emission transition in silicone single crystals. *Phys Rev Lett*, 104(235502-1):1–4.

Shah, K., Zhao, Y., and Kohli, D. (2010). Development of a universal resin rich peel ply for composite bonding applications. In *International SAMPE Technical Conference (Proceedings)*, Salt Lake City, USA. October 11-14.

Sharma, P. and Ganti, S. (2004). Size-dependent eshelby's tensor for embedded nano-inclusions incorporating surface/interface energies. *J Appl Mech, Transactions ASME*, 71(5):663–671.

Shbeeb, N. and Binienda, W. (1999). Analysis of an interface crack for a functionally graded strip sandwiched between two homogeneous layers of finite thickness. *Eng Fract Mech*, 64(6):693–720.

Shih, Y.-F. and Jeng, R.-J. (2004). IPNs based on unsaturated polyester/epoxy: IV. investigation on hydrogen bonding, compatability and interaction behavior. *Polym Int*, 53(11):1892–1898.

Skal's'kyi, V., Andreikiv, O., and Serhienko, O. (2003). Investigation of the plastic deformation of materials by the acoustic emission method (review). *Mater Sci*, 39(1):86–107.

Skrifvars, M., Berglund, L., and Ericson, M. (1999). Microscopy of the morphology in low styrene emission glass fiber/unsaturated polyester laminates. *J Appl Polym Sci*, 71(10):1555–1562.

Song, J., Kostka, A., Veehmayer, M., and Raabe, D. (2011). Hierarchical microstructure of explosive joints: Example of titanium to steel cladding. *Mater Sci Eng A*, 528(6):2641–2647.

Sperling, L. (2006). *Introduction to physical polymer science*, chapter Polymer surfaces and interfaces, pages 613–686. Wiley, Hoboken, USA.

Sturiale, A., Vázquez, A., Cisilino, A., and Manfredi, L. (2007). Enhancement of the adhesive joint strength of the epoxy amine system via the addition of a resole type phenolic resin. *Int J Adhes Adhes*, 27(1):156–164.

Sugimura, Y., Grondin, L., and Suresh, S. (1995). Fatigue crack growth at arbitrary angles to bimaterial interfaces. *Scripta Metall Mater*, 33(12):2007–2012.

Sun, X. and Davidson, B. (2005). A direct energy balance approach for determining energy release rates in three and four point bend end notched flexure tests. *Int J Fract*, 135(1-4):51–72.

Suo, Z. and Hutchinson, J. (1990). Interface crack between two elastic layers. *Int J Fract*, 43(1):1–18.

Tan, H. (2002). *Comprehensive structural integrity*, chapter Combined atomistic and continuum simulation of fracture and corrosion, pages 1–39. Elsevier Science, Oxfordshire, UK.

Tilbrook, M., Reimanis, I., Rozenburg, K., and Hoffman, M. (2005). Effects of plastic yielding on crack propagation near ductile/brittle interfaces. *Acta mater*, 53(14):3935–3949.

Tilbrook, M., Rozenburg, K., Steffler, E., Rutgers, L., and Hoffman, M. (2006). Crack propagation paths in layered, graded composites. *Compos Part B Eng*, 37(6):490–498.

Timoshenko, S. (1925). Analysis of bi-metal thermostats. *J Opt Soc Am*, 11(1):233–255.

Towashiraporn, P., Subbarayan, G., and Desai, C. (2005). A hybrid model for computationally efficient fatigue fracture simulations at microelectronic assembly interfaces. *Int J Solids Struct*, 42(15):4468–4483.

Trädegård, A., Nilsson, F., and Östlund, S. (1998). FEM-remeshing technique applied to crack growth problems. *Comput Methods Appl Mech Eng*, 160(1-2):115–131.

Traiviratana, S., Bringa, E., Benson, D., and Meyers, M. (2008). Void growth in metals: atomistic calculations. *Acta mater*, 56:3874–3886.

Tsai, M. and Morton, J. (1995). The effect of a spew fillet on adhesive stress distributions in laminated composite single-lap joints. *Compos Struct*, 32(1-4):123–131.

Tvergaard, V. and Hutchinson, J. (2009). Analyses of crack growth along interface of patterned wafer-level cu-cu bonds. *Int J Solids Struct*, 46(18-19):3433–3440.

Van Oss, C. (1987). Monopolar surfaces. *Adv Colloid Interface Sci*, 28:35–64.

Van Oss, C. (1988). Interfacial Lifshitz-van der Waals and polar interactions in macroscopic systems. *Chem Rev*, 88:927–941.

Van Rooijen, R., Sinke, J., and Van Der Zwaag, S. (2005). Improving the adhesion of thin stainless steel sheets for fibre metal laminate (FML) applications. *J Adhes Sci Technol*, 19(16):1387–1396.

Wang, H. and Turner, J. (2008). Austenitic stainless steels in high temperature phosphoric acid. *J Power Sourc*, 180(2):803–807.

Wübbenhorst, M. and Lupascu, V. (2005). Glass transition effects in ultra-thin polymer films studied by dielectric spectroscopy – chain confinement vs. finite size effects. In *International Symposium on Electrets (Proceedings)*, Salvador, Brazil. September 11-14.

Yang, F. and Pitchumani, R. (2004). Effects of interphase formation on the modulus and stress concentration factor of fiber-reinforced thermosetting-matrix composites. *Compos Sci Technol*, 64(10-11):1437–1452.

Yu, Y., Ashcroft, I., and Swallowe, G. (2006). An experimental investigation of residual stresses in an epoxy-steel laminate. *Int J Adhes Adhes*, 26(7):511–519.

Zavattieri, P., Hector Jr., L., and Bower, A. (2007). Determination of the effective mode-I toughness of a sinusoidal interface between two elastic solids. *Int J Fract*, 145(3):167–180.

Zavattieri, P., Hector Jr., L., and Bower, A. (2008). Cohesive zone simulations of crack growth along a rough interface between two elastic-plastic solids. *Eng Fract Mech*, 75(15):4309–4332.

Zhang, X. and Sharma, P. (2005). Inclusions and inhomogeneities in strain gradient elasticity with couple stresses and related problems. *Int J Solids Struct*, 42(13):3833–3851.

Composite and hybrid materials are gaining ground among the traditional engineering materials in load carrying applications. The mechanical performance of these new materials relies on the strength of interfaces between several dissimilar components. This dissertation sheds light on the experimental observation, numerical simulation and fundamental definition of interface strength on a micro scale. Engineering toughening factor is developed to unite macro and micro length scales. Although being a straightforward relation, the determination of an engineering toughening factor for a practical interface necessitates sophisticated fracture testing and interface modelling, like is presented in the dissertation.

Aalto-DD 151/2014

ISBN 978-952-60-5890-0
ISBN 978-952-60-5891-7 (pdf)
ISSN-L 1799-4934
ISSN 1799-4934
ISSN 1799-4942 (pdf)

Aalto University

Department of Applied Mechanics
www.aalto.fi

BUSINESS + ECONOMY

ART + DESIGN + ARCHITECTURE

SCIENCE + TECHNOLOGY

CROSSOVER

DOCTORAL DISSERTATIONS